Influence of Monovalent Cation Identity on Parvalbumin Divalent Ion-Binding Properties†

Michael T. Henzl,* John D. Larson, and Sayeh Agah

Department of Biochemistry, University of Missouri—Columbia, Columbia, Missouri 65211

Received October 21, 2003; Revised Manuscript Received December 23, 2003

ABSTRACT: Rat α- and *β*-parvalbumins have distinct monovalent cation-binding properties [Henzl et al. (2000) *Biochemistry 39*, 5859−5867]. *β* binds two Na^+ or one K^+, and α binds one Na^+ and no K^+. Ca^{2+} abolishes these binding events, suggesting that the monovalent ions occupy the EF-hand motifs. This study compares α and *β* divalent ion affinities in Na^+ and K^+ solutions. Solvent cation identity seriously affects α. In Hepes-buffered NaCl, at 5 °C, the macroscopic Ca^{2+}-binding constants are 2.6×10^8 and 6.4×10^7 M^{-1} and the Mg^{2+} constants, 1.8×10^4 and 4.3×10^3 M^{-1}. In Hepes-buffered KCl, the Ca^{2+} values increase to 2.9×10^9 and 6.6×10^8 M^{-1} and the Mg^{2+} values to 2.2×10^5 and 3.7×10^4 M^{-1}. Monte Carlo simulation of α binding data—employing site-specific constants and explicitly considering Na^+ binding—yields a K_{Na} of 630 M^{-1} and indicates that divalent ion-binding is positively cooperative. NMR data suggest that the lone Na^+ ion occupies the CD loop. Solvent cation identity has a smaller impact on *β*. In Na^+, the Ca^{2+} constants for the EF and CD sites are 2.3×10^7 and 1.5×10^6 M^{-1}, respectively; the Mg^{2+} constants are 9.2×10^3 and 1.7×10^2 M^{-1}. In K^+, these values shift to 3.1×10^7 and 3.8×10^6 M^{-1} and the latter to 1.4×10^4 and 2.9×10^2 M^{-1}. These data suggest that parvalbumin divalent ion affinity, particularly that of rat α, can be significantly attenuated by increased intracellular Na^+ levels.

Transient alterations in cytosolic Ca^{2+} levels influence myriad biological processes (*1*, *2*). Variations in location, amplitude, duration, and frequency permit diverse phenomena to be regulated by the same second messenger. These Ca^{2+} signals—produced by the action of Ca^{2+} channels and ATP-driven Ca^{2+} pumps—can be further modulated by various Ca^{2+}-binding proteins.

"EF-hand"[1] proteins (*3*−*6*) participate in virtually all Ca^{2+}-signaling pathways. This protein family is named for its characteristic helix-loop-helix Ca^{2+}-binding motif—the configuration of which can be mimicked by the thumb, index finger, and forefinger of the right-hand. Within the binding loop, the bound Ca^{2+} ion is coordinated by seven oxygen ligands arranged in a pentagonal bipyramidal manner (Figure 1A). The EF-hand family includes more than 250 members, divided into 45 subfamilies. Certain of these proteins, for example, calmodulin and troponin C, function as Ca^{2+}-dependent regulatory proteins; others, such as calbindin and parvalbumin, serve as Ca^{2+} buffers.

The parvalbumins (*3*−*7*) were the first EF-hand family members detected, purified, sequenced, and crystallized. These small (M_r 12 000), vertebrate-specific proteins contain two EF-hand motifs, called the CD and EF sites, and the nonbinding remnant of a third, the AB domain (Figure 1B). Parvalbumin physical studies have contributed significantly to our knowledge of EF-hand function. In fact, the crystal structure of carp parvalbumin established the EF-hand structural paradigm (*8*).

The parvalbumin family includes α and *β* sublineages (*9*), distinguished by isoelectric point (*β* < 5), C-terminal helix length (typically one residue shorter in *β*), and several lineage-specific sequence assignments. Mammals express one isoform from each lineage (*10*). Particularly abundant in fast-twitch skeletal muscle, the α isoform is also expressed in a variety of other specialized cell types—notably rapidly firing neurons (*11*−*13*) and the *inner hair cells* of the organ of Corti (*14*), the mammalian auditory organ. The distribution of the *β* isoform, also known as oncomodulin, is far more limited, with expression in postnatal mammals apparently restricted to the *outer hair cells* of the organ of Corti (*15*, *16*).

The selective recruitment of α and *β* by the two sensory cell types in the auditory organ may have been dictated by their disparate metal ion-binding properties. Whereas the α CD and EF sites are both high-affinity sites (*17*−*19*), the CD site in *β* is a low-affinity site (*20*, *21*). An explanation for this functional diversity—in proteins exhibiting 49% sequence identity (*22*, *23*)—could provide welcome insight into EF-hand structure−affinity relationships.

† This work was supported by NSF Awards MCB9603877 and MCB0131166 (to M.T.H.).

* Author to whom correspondence should be addressed [telephone (573) 882-7485; fax (573) 884-4812; e-mail henzlm@missouri.edu].

[1] CD site, parvalbumin metal ion-binding site flanked by the C and D helical segments; DSC, differential scanning calorimetry; EDTA, ethylenediaminetetraacetic acid; EF site, parvalbumin metal ion-binding site flanked by the E and F helical segments; EGTA, ethylene glycol bis(*β*-aminoethyl ether)-*N*,*N*,*N*′,*N*′-tetraacetic acid; FAAS, flame atomic absorption spectrometry; Hepes, 4-(2-hydroxyethyl)-1-piperazineethanesulfonic acid; HSQC, heteronuclear single-quantum coherence; ITC, isothermal titration calorimetry; NLLS, nonlinear least squares; NMR, nuclear magnetic resonance; P_i, phosphate; PV, parvalbumin.

10.1021/bi035890k CCC: $27.50
Published on Web 02/18/2004

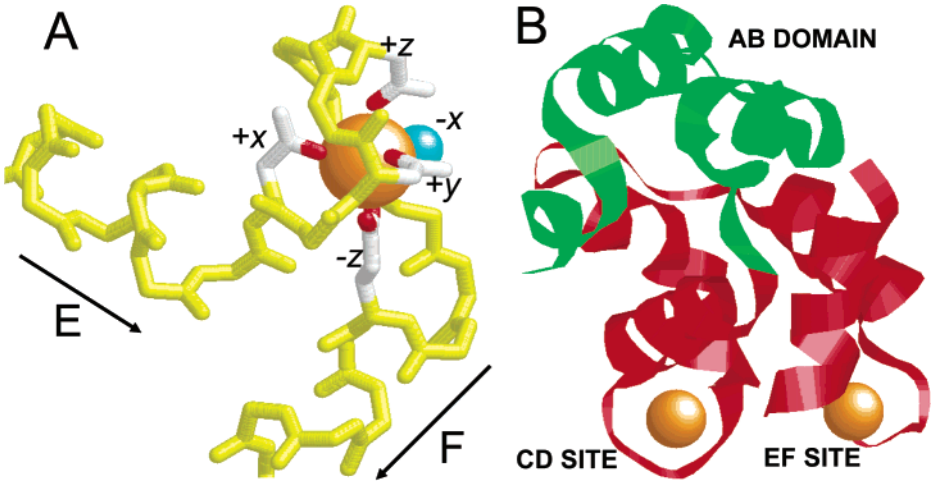

FIGURE 1: (A) Canonical EF-hand metal ion-binding motif, showing the pseudo-octahedral arrangement of ligands around the bound Ca^{2+}. The coordination of the glutamyl residue at $-z$ is bidentate, so that the ligand geometry is actually pentagonal bipyramidal. A water molecule (cyan) occupies the $-x$ position. The $-y$ ligand, an invariant main-chain carbonyl, is obscured in this view. (B) Rat β-parvalbumin tertiary structure, produced from the 1RRO PDB file. The N-terminal AB domain (residues 1−39) occludes the hydrophobic face of the CD−EF metal ion-binding domain, preventing calmodulin-like interactions with amphipathic helical peptides.

Due to their lower electrostatic free energy and increased opportunities for tertiary interactions, α-parvalbumins are expected to display inherently greater thermodynamic stability. However, the Ca^{2+}-free rat α isoform is substantially *less* stable than rat β at physiologically relevant ionic strength (*24*). The atypical stability of rat β was recently traced to Pro-21 and Pro-26 (*25*). Prior to this discovery, however, the influence of monovalent cation identity and concentration on conformational stability was investigated (*26*).

Although the β isoform retains its superior stability over the entire ionic strength range examined, these studies revealed a differential interaction between the Ca^{2+}-free proteins and solvent cations. At pH 7.4 and a cation concentration of 0.2 M, the apparent Na^+ binding capacity of β approaches 2 equiv, and the K^+ binding capacity approaches 1 equiv. In contrast, α apparently binds a single equivalent of Na^+ and exhibits negligible affinity for K^+. Binding of the monovalent cations, monitored by isothermal titration calorimetry (ITC), is abolished in the presence of 100 μM Ca^{2+}. This finding suggests that the bound monovalent ions reside in the EF-hand binding loops. Thus, parvalbumin divalent ion affinities may be shaped, in part, by monovalent ion-binding capacity and affinity. To address this issue, we have examined the Ca^{2+}- and Mg^{2+}-binding properties of rat α- and β-parvalbumins in Na^+- and K^+-containing buffers.

For the α isoform in K^+ solution, this undertaking was complicated by two factors: very high Ca^{2+} affinity and marginal conformational stability. The protein's avidity for Ca^{2+} made the production of apoprotein difficult. It also precluded the use of flow dialysis and necessitated the development of an ITC-based method for determining binding constants. Because the apoprotein is partially denatured at 25 °C (*26*), metal ion-binding is linked to folding, so that ITC data collected at 25 °C are not amenable to analysis with a simple two-site binding model. To circumvent this difficulty, the influence of Na^+ and K^+ on α divalent ion-binding behavior was investigated at 5 °C. However, the binding constants have also been measured in Na^+ at 25 °C, to gauge the impact of temperature on the free energy of divalent ion binding.

The apparent Ca^{2+}- and Mg^{2+}-binding constants for α were used to extract binding curves from ITC experiments conducted in Na^+ and K^+ solutions. The resulting datasets were subjected to global Monte Carlo simulation, employing models that explicitly included the monovalent cation-binding event. These analyses yielded an estimate for the Na^+-binding constant.

MATERIALS AND METHODS

$^{45}CaCl_2$ was purchased from Perkin-Elmer Life Sciences, $^{15}NH_4Cl$ from Isotec, D_2O from Sigma-Aldrich Co., and Celtone-N from Spectra Stable Isotopes. Spectrapor 1 dialysis membrane (MWCO 6000−8000), ScintiSafe Econo 2 scintillation cocktail, nitric acid, NaCl, KCl, Hepes (free acid), NaOH, KOH, $CaCl_2 \cdot 2H_2O$, $MgCl_2 \cdot 2H_2O$, and $Na_2EDTA \cdot 2H_2O$ were obtained from Fisher. EDTA (free acid) was purchased from Sigma-Aldrich. All Ca^{2+} and Mg^{2+} titrant concentrations were determined by ITC, titrating gravimetrically prepared standard solutions of EDTA.

Protein Expression and Purification. The expression and isolation of recombinant rat α- and β-parvalbumins have been described previously (*20*, *24*). Because the proteins are devoid of tryptophan, the A_{292} value provides a useful criterion of homogeneity. Employing an average mass absorptivity at 292 nm of 0.5 $(mg/mL)^{-1}$ cm^{-1} for the contaminants, the estimated purity of the protein preparations used for this work exceeded 98%. Protein concentrations were estimated spectrophotometrically, employing extinction coefficients of 1600 and 3260 M^{-1} cm^{-1} for rat α and β, respectively.

Divalent metal ions were removed from the protein preparations prior to binding analyses by passage over EDTA-derivatized agarose at 4 °C. The chelating matrix prepared according to the method of Haner et al. (*27*) proved to be inadequate for complete removal of Ca^{2+} from the α isoform. However, a substantially higher binding capacity (≥25 μmol/mL gel) can be achieved by a modification of the preparative method, described elsewhere (*28*). Provided that the chromatography is conducted in Na^+-containing buffer, using 2 mL of gel/mg of protein, this material reduces

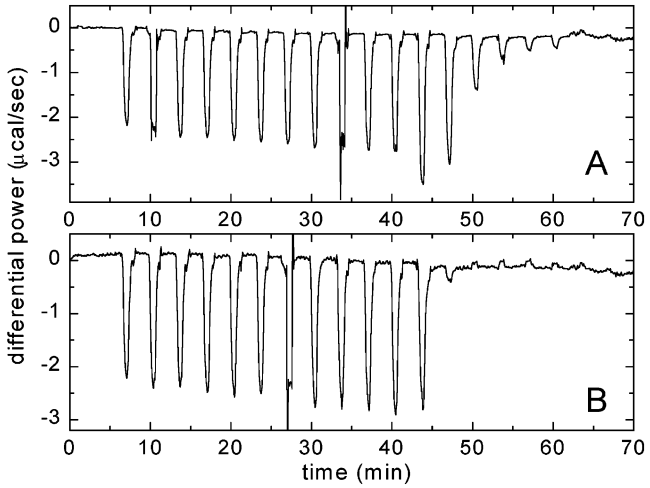

FIGURE 2: Susceptibility of Ca^{2+}-free rat α to modification. (A) 3.0 mM Ca^{2+} vs 195 μM Ca^{2+}-free rat α. Residual Ca^{2+} had been removed from the protein by EDTA−agarose chromatography at 23 °C. (B) 3.0 mM Ca^{2+} vs 185 μM Ca^{2+}-free α. Treatment of this protein sample with EDTA−agarose was conducted at 4 °C. Both titrations were performed at 25 °C, in 0.15 M NaCl and 0.025 M Hepes−NaOH, pH 7.4.

the residual Ca^{2+} content—measured by flame atomic absorption spectrometry (FAAS)—to <0.02 equiv. The extremely high Ca^{2+} affinity of α in K^+ solution prevented direct removal of the divalent cation. Instead, Ca^{2+} removal was carried out in Na^+ solution, whereupon the Na^+ was exchanged for K^+ by repeated rounds of concentration and dilution with Ca^{2+}-free K^+-containing buffer.

Ca^{2+}-free α is susceptible to oxidation, particularly in K^+-containing solution. This modification is readily apparent in calorimetrically monitored titrations with Ca^{2+}, manifested by significant perturbations of binding enthalpy and affinity. The titration depicted in Figure 2A was conducted with protein that had been subjected to EDTA−agarose chromatography at room temperature. Notice the sharp increase in binding heat near the equivalence point and the gradual return of the binding heats to baseline values. This behavior can be prevented by performing all manipulations of the apoprotein at 0−4 °C. The titration displayed in Figure 2B was conducted with protein treated with EDTA−agarose at 4 °C. The abrupt increase in binding heat near the end of the titration has been eliminated, and the binding heats return to the baseline immediately after the equivalence point. DSC analyses suggest that Ca^{2+}-free α is partially unfolded at 25 °C (*26*). It is possible that the solvent accessibility of one or more methionyl residue is increased under these conditions. The rat α sequence lacks cysteine.

Flow-dialysis measurements were performed as described by Womack and Colowick (*29*), with minor modifications. After assembly of the flow-dialysis cell, the lower chamber is rinsed with 1% HNO_3, then with deionized water, and finally with the appropriate Ca^{2+}-free buffer, at a flow rate of 2.0 mL/min. During this period, the upper chamber is subjected to a similar manual rinsing procedure. A 0.50 mL sample of protein (100 μM)—containing roughly 3 μC_i of $^{45}Ca^{2+}$—is then introduced into the upper chamber. Following an equilibration period (30−120 min), 2.0 μL aliquots of titrant (each containing 5.0 nmol of Ca^{2+}) are added to the samples at 8 min intervals. Five minutes after each titrant addition, a 3.0 mL sample of the eluate is collected for liquid scintillation analysis. When the titration endpoint is reached, signaled by an abrupt increase in the eluate radioactivity, 10 μL of 1.0 M Ca^{2+} is added to the sample. The large molar excess of nonradioactive Ca^{2+} liberates essentially all of the $^{45}Ca^{2+}$. The resulting level of radioactivity in the eluate—commensurate with 100% free Ca^{2+}—permits the free Ca^{2+} concentration to be calculated at each point in the titration. Knowing the total Ca^{2+} values, the concentration of bound Ca^{2+} can be calculated by difference. Samples were typically counted for 20 min in a Beckman LS6500 liquid scintillation counter.

Experiments were conducted at 25 °C, at pH 7.4, in 0.15 M NaCl and 0.025 M Hepes−NaOH or in 0.15 M KCl and 0.025 M Hepes−KOH. In each buffer system, titrations were performed in the absence of Mg^{2+} and at fixed levels of the competing ion. The data were satisfactorily accommodated by an independent two-site model

$$\bar{X} = \frac{k_1[Ca^{2+}]}{1 + k_1[Ca^{2+}] + k_{1M}[Mg^{2+}]} + \frac{k_2[Ca^{2+}]}{+1 + k_2[Ca^{2+}] + k_{2M}[Mg^{2+}]} \quad (1)$$

where k_1 and k_2 represent the microscopic Ca^{2+}-binding constants and k_{1M} and k_{2M} the corresponding Mg^{2+} constants. The free Ca^{2+} concentration at each point is determined from the level of radioactivity in the eluate, and the extent of binding ($\bar{X}$) is obtained by dividing the concentration of bound Ca^{2+}—the difference between the total and free Ca^{2+} levels—by the total protein concentration. For experiments conducted with Mg^{2+} present, the free concentration of the competing ion is estimated by bisection (*30*), employing the free Ca^{2+} level, the total Mg^{2+} concentration, and the current estimates of the Ca^{2+}- and Mg^{2+}-binding constants.

The data from experiments with and without Mg^{2+} were compiled into a single dataset, which was then analyzed by weighted nonlinear least-squares minimization. This composite dataset includes columns for $\bar{X}$, the estimated standard deviation, the free Ca^{2+} concentration, the total Ca^{2+} concentration, the total Mg^{2+} concentration, an experiment number, and the data point number within that experiment. The global analysis program, developed in-house, employs the CURFIT algorighm in the original Bevington monograph (*31*). Supplied with $\bar{X}$, the free levels of Ca^{2+} and Mg^{2+}, and the standard deviation for each experimental point, the program returns estimates for the Ca^{2+}- and Mg^{2+}-binding constants that yield the lowest reduced chi-square value (χ_ν^2) for the composite dataset:

$$\chi_\nu^2 = \frac{\chi^2}{\nu} = \frac{1}{\nu}\sum_i \left[\frac{y_i - y(x_i)}{\sigma_i}\right]^2 \quad (2)$$

In this expression, ν represents the degrees of freedom, y_i and $y(x_i)$ denote the observed and calculated values of $\bar{X}$ for the ith data point, and σ_i is the estimated standard deviation for that point. The σ_i values ranged from 0.05 early in the titration to 0.01 near the end. In the absence of positive cooperativity, the microscopic (k_1, k_2) constants are mathematically related to the macroscopic binding constants (K_1, K_2) reported in Table 2 as follows:

$$K_1 = k_1 + k_2; \quad K_2 = k_1k_2/(k_1 + k_2) \tag{3}$$

Conversely, given values for K_1 and K_2, the apparent values of k_1 and k_2 are equal to

$$k_1 = \frac{K_1 + \sqrt{K_1^2 - 4K_1K_2}}{2}$$
$$k_2 = \frac{K_1 - \sqrt{K_1^2 - 4K_1K_2}}{2} \tag{4}$$

After identification of the optimal parameter values and the lowest chi-square, χ^2(min), confidence intervals were determined by incrementing the parameter of interest, fixing its value, and repeating the least-squares minimization, allowing the remaining parameters to vary. This procedure was repeated until the chi-square value, χ^2(par), exceeded a specified threshold, given by

$$\chi^2(\text{par}) = \left(1 + \frac{p}{\nu}F(p,\nu,P)\right)(\chi^2(\text{min})) \tag{5}$$

In eq 5, p is the number of fitting parameters, ν the degrees of freedom, P the probability that the increase in χ^2 could be the result of random errors (0.32 for the 68% confidence limit), and $F(p,\nu,P)$ the corresponding F statistic (*32*). We utilized the values of $F(p,\nu,P)$ tabulated by Lacowicz (*33*). After the upper limit had been determined, the parameter value was decremented from its optimal value until χ^2(par) again exceeded the specified threshold.

Isothermal Titration Calorimetry. With the exception of the data presented in Figure 2, all experiments were conducted in a VP-ITC calorimeter (MicroCal, Inc.). Following thermal equilibration, additions of titrant were made, at 180 s intervals, to the 1.41 mL protein samples. To facilitate comparison with the flow-dialysis data, experiments were likewise conducted at pH 7.4, in 0.15 M NaCl and 0.025 M Hepes−NaOH or in 0.15 M KCl and 0.025 M Hepes−KOH. For each buffer system, titrations were carried out with Ca^{2+} alone, Mg^{2+} alone, Ca^{2+} at several fixed levels of Mg^{2+}, Ca^{2+} in the presence of EDTA, Ca^{2+} in the presence of EGTA, and usually Mg^{2+} in the presence of EDTA. After subtraction of the baseline heats, the experiments were compiled into a master data file. This composite dataset was then subjected to global nonlinear least-squares analysis, as described in detail elsewhere (*34*). With the exception of the initial point in each titration, a uniform standard deviation (0.35 μcal per addition) was assumed for all data points. This value reflects the standard deviation measured with our instrument for repeated additions of 1.0 mM Ca^{2+} into excess EDTA, in 0.15 M NaCl and 0.025 M Hepes−NaOH, pH 7.4. Initial titration points are invariably unreliable, due to diffusion of titrant from the buret tip during the thermal equilibration period, and were assigned uncertainties of 10^7, to ensure that they received no weight during the fitting process.

The uncertainties associated with the ITC analyses were evaluated by inspection of the parameter correlation matrices, evaluation of the 68% confidence intervals, and Monte Carlo simulations (*34*).

The titrations displayed in Figure 2 were conducted at 25 °C with a model 4209 microtitration calorimeter from Calorimetry Sciences Corp., making 10 μL additions at 200 s intervals to 1.00 mL protein samples.

NMR Spectroscopy. Rat α-PV was produced in *Escherichia coli* DH5α harboring pLD2, a derivative of pBluescript (Stratagene). To achieve uniform ^{15}N labeling, the bacteria were cultured on M9 minimal medium containing 1.25 g/L $^{15}NH_4Cl$, 2.5 g/L glucose, trace metals, MEM vitamins, and 2.5% (v/v) Celtone-N. Each liter of culture yielded ~10 mg of protein. Purity exceeded 98%, based on UV absorbance and SDS−polyacrylamide gel electrophoresis.

Ca^{2+} was removed from the protein samples prior to NMR analysis by passage over EDTA-derivatized agarose in 0.15 M NaCl and 0.005 M Mes−NaOH, pH 7.4, at 4 °C. When required, the Na^+ was exchanged for K^+ by repeated concentration and dilution in an Amicon ultrafiltration cell (YM10 membrane), employing Ca^{2+}-free 0.15 M KCl and 0.005 M Mes−KOH, pH 7.4. As explained above, this strategy was dictated by the extremely high Ca^{2+} affinity of α in K^+-containing solution. After verification, by FAAS, that >98% of the Ca^{2+} had been removed, the pH was adjusted to 6.0; D_2O (containing 0.15 M NaCl or KCl, as appropriate) was added to a final concentration of 10% (v/v), the sample volume was reduced to 0.60 mL, and the sample was placed in a 5 mm NMR tube (Kontes).

NMR spectroscopy was conducted at 25 °C on a Varian Unity-600 spectrometer. ^1H chemical shifts were referenced to the methyl protons of TSP (0 ppm); ^{15}N shifts were referenced to acidic NH_4Cl at 25 °C (24.93 ppm). ^1H,^{15}N-HSQC spectra were acquired with a pulse program based on that of Mori et al. (*35*). Amide proton and nitrogen assignments have been previously reported for the Ca^{2+}-bound protein (*36*). Assignments for select residues in the Ca^{2+}-free samples were verified by inspection of TOCSY−HSQC (*37*) and NOESY−HSQC (*38*) experiments.

Estimation of Rat α Monovalent Cation Affinity by Monte Carlo Simulation. Binding curves were extracted from select ITC experiments conducted in the presence of Na^+ or K^+. Estimates of the Na^+ affinity constants for rat α were obtained by Monte Carlo analysis, employing a model that includes these macroscopic species: M, MX, MX_2, MY, and MXY—where M represents the macromolecule, X the relevant divalent ion, and Y the major solvent cation. Mathematically, the extent of divalent ion-binding, $\bar{X}$, for this system is described by

$$\bar{X}_i = (K_{10} \times (1 + K_{11} \times Y_i) \times X_i + 2 \times K_{20}K_{10} \times X_i^2)/P \tag{6}$$

where P is the relevant partition function, equal to

$$P = 1 + K_{01} \times Y_i + K_{10} \times (1 + K_{11}Y_i) \times X_i + K_{20}K_{10}X_i^2 \tag{7}$$

In these equations, K_{10} and K_{20} are the macroscopic association constants for the first and second divalent ion-binding events, K_{01} is the corresponding monovalent ion-binding constant, and K_{11} is the monovalent ion-binding constant for the MXY species.

The divalent ion-binding constants determined for α in K^+ solution provided values for K_{10} and K_{20}. Calorimetrically monitored titrations of α with Na^+, reported previously (*26*), yielded a starting estimate for the Na^+-binding constant, K_{01}.

Table 1: α- and β-PV Divalent Ion-Binding Properties

protein	solvent cation	T (°C)	Ca^{2+} values				Mg^{2+} values			
			K_1[a] (M^{-1})	H_1 (kcal/mol)	K_2 (M^{-1})	H_2 (kcal/mol)	K_{1M} (M^{-1})	H_{1M} (kcal/mol)	K_{2M} (M^{-1})	H_{2M} (kcal/mol)
Isothermal Titration Calorimetry										
β-PV	Na^+	25	2.45×10^7	−4.10	1.43×10^6	−3.46	9.40×10^3	3.01	1.64×10^2	4.16
			(2.20, 2.71)	(−4.16, −4.06)	(1.29, 1.61)	(−3.52, −3.41)	(9.10, 9.83)	(2.97, 3.05)	(1.54, 1.75)	(4.00, 4.32)
	K^+	25	3.45×10^7	−5.49	3.36×10^6	−3.43	1.40×10^4	2.02	2.80×10^2	5.15
			(3.73, 3.18)	(−5.55, −5.43)	(3.60, 3.10)	(−3.48, −3.36)	(1.51, 1.29)	(2.08, 1.94)	(3.13, 2.52)	(5.32, 4.99)
α-PV	Na^+	25	2.50×10^8	−1.34	6.24×10^7	−4.30	3.66×10^4	7.92	9.02×10^3	0.24
			(2.65, 2.37)	(−1.40, −1.28)	(6.60, 5.92)	(−4.36, −4.18)	(3.81, 3.52)	(8.00, 7.83)	(9.38, 8.68)	(0.30, 0.17)
	Na^+	5	2.55×10^8	−1.41	6.36×10^7	−4.05	1.76×10^4	7.82	4.30×10^3	1.63
			(2.74, 2.41)	(−1.46, −1.35)	(6.82, 6.00)	(−4.11, −3.97)	(1.88, 1.67)	(7.91, 7.73)	(4.58, 4.08)	(1.71, 1.55)
	K^+	5	2.94×10^9	−3.64	6.59×10^8	−4.22	2.17×10^5	4.42	3.71×10^4	2.29
			(3.31, 2.51)	(−3.75, −3.58)	(7.40, 5.62)	(−4.29, −4.16)	(2.40, 2.00)	(4.48,4.35)	(4.12, 3.42)	(2.38, 2.22)
Flow Dialysis										
β-PV	Na^+	25	2.27×10^7		1.05×10^6		1.23×10^4		7.4	
			(2.22, 2.32)		(1.03, 1.07)		(1.20, 1.26)		(0, 15)	
	K^+	25	3.05×10^7		3.50×10^6		1.73×10^4		3.99×10^2	
			(2.99, 3.11)		(3.42, 3.59)		(1.68, 1.77)		(3.70, 4.27)	
α-PV	Na^+	25	1.74×10^8		4.27×10^7		3.71×10^4		4.97×10^3	
			(1.67, 1.80)		(3.97, 4.59)		(3.54, 3.90)		(4.55, 5.39)	

[a] The reported uncertainties (values in parentheses) reflect the 68% confidence intervals.

K_{11} was arbitrarily set to 1. After calculation of an initial χ^2 value, a new parameter set was generated by incrementing each binding constant by an arbitrary quantity, ΔK. The magnitude of ΔK is equal to the output from a random number generator multiplied by some arbitrary fraction of the initial parameter value (δ). χ^2 is then recalculated.

Simulations can be performed both with and without minimization. The objective in the latter case is merely to collect parameter sets satisfying an arbitrary χ^2 criterion. For this application, δ is typically set to a fairly large value (e.g., 0.1), and a large number (e.g., 10 000) of parameter sets are accumulated. The parameter values associated with the lowest χ^2 serve as the starting point for minimization. When χ^2 is minimized, an acceptable parameter set must return a χ^2 value below the current one—in which case it then serves as a basis for further simulation. The program is allowed to run until no further decrease in χ^2 is observed. The δ values employed for minimization are typically quite small (e.g., 0.001), to help ensure that the parameter values remain in the vicinity of the nearby minimum. In practice, it is necessary to employ both modes (i.e., with and without minimization) iteratively, to obtain satisfactory agreement between the observed and calculated values—particularly when the starting parameter values are far from a solution.

The α data were also analyzed with a model that employed site-specific binding constants and included these microscopic species: M, XM, MX, XMX, YM, and YMX. The extent of binding for this system is given by the equation

$$\bar{X}_i = ((k_1 + k_2) \times X_i + 2c_{12}k_2k_1 \times X_i^2 + k_{Na}k_2 \times X_i \times Y_i)/P \quad (8)$$

where P, the partition function, equals

$$P = 1 + (k_1 + k_2) \times X_i + c_{12}k_2k_1 \times X_i^2 + k_{Na} \times Y_i + k_{Na}k_2 \times X_i \times Y_i \quad (9)$$

k_1 and k_2 are the microscopic binding constants for site 1 and site 2, respectively, and c_{12} is a cooperativity coefficient. Occupation of site 1 or 2 is indicated by placement of X; that is, XM implies binding of the divalent ion at site 1 and MX, binding at site 2. Note that this model assumes that Y, the monovalent ion, binds exclusively to site 1. For complete generality, a cooperativity coefficient could have been included for formation of the YMX species. Because agreement between calculated and observed values of $\bar{X}$ was obtained without the additional parameter, it was omitted.

RESULTS

In the following paragraphs, the divalent ion affinities of rat α- and β-parvalbumins are compared in buffers containing Na^+ or K^+. Whereas it was possible to study β by flow dialysis and titration calorimetry at 25 °C, heightened Ca^{2+} affinity frustrated attempts to study α by flow dialysis in K^+ solution. The marginal stability of α in K^+-containing buffers further complicated the analysis, so that ultimately the comparison of α divalent ion affinity in Na^+ and K^+ was conducted at 5 °C.

Affinity of Rat β for Ca^{2+} and Mg^{2+} in Na^+- and K^+-Containing Solutions

Flow Dialysis. The Ca^{2+} affinities of the β CD and EF sites are well suited to determination by $^{45}Ca^{2+}$ flow dialysis. For this study, samples of rat β were titrated with Ca^{2+} in the absence of Mg^{2+} and at five levels of the competing ion. The combined data from these six titrations were subjected to weighted global least-squares minimization. This procedure was conducted in both Na^+- and K^+-containing buffer solutions. Data for the two series of experiments are plotted in panels A and B, respectively, of Figure 3, the solid lines indicating the optimal least-squares fit for the composite dataset. The resulting parameter estimates and 68% confidence intervals are presented in Table 1.

The values of the Ca^{2+}-binding constants determined in Na^+-containing solution—2.27×10^7 and 1.05×10^6 M^{-1}—agree well with previous estimates, obtained from the analysis of single experiments (*39*). However, the Mg^{2+} constants—12 300 and 7 M^{-1}—are substantially different.

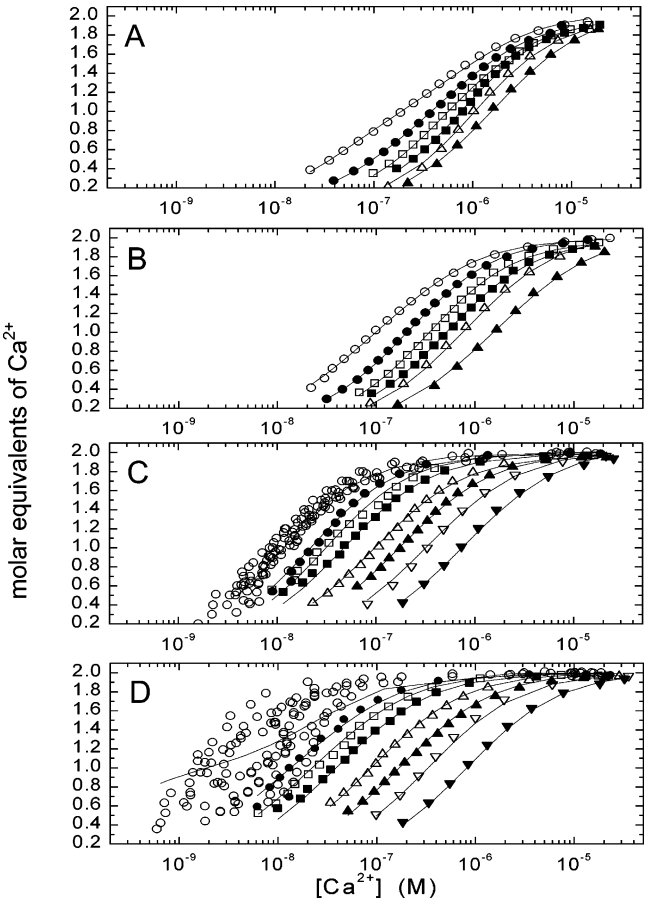

FIGURE 3: $^{45}Ca^{2+}$ flow-dialysis measurements on rat α and β in Na^+ and K^+ solution. (A) Titration of β with Ca^{2+} in 0.15 M NaCl and 0.025 M Hepes−NaOH, pH 7.40, in the absence or presence of fixed levels of Mg^{2+}. Mg^{2+} concentrations: 0 (○); 0.20 mM (●); 0.50 mM (□); 1.0 mM (■); 2.0 mM (△); 5.0 mM (▲). (B) Titration of β in 0.15 M KCl and 0.025 M Hepes−KOH, pH 7.40. The competing Mg^{2+} concentrations were identical to those listed for panel A. (C) Titration of α in NaCl/Hepes, in the absence and presence of fixed levels of Mg^{2+}. Mg^{2+} concentrations: 0 (○); 0.05 mM (●); 0.10 mM (□); 0.20 mM (■); 0.50 mM (△); 1.0 mM (▲); 2.0 mM (▽); 5.0 mM (▼). (D) Titration of α in KCl/Hepes. Competing Mg^{2+} concentrations were identical to those listed for panel C.

Although the values reported here are inherently more reliable, being the product of a global least-squares fit, the significance of the second binding constant is nevertheless questionable. The highest competing level of Mg^{2+} employed in this study, 5.0 mM, would not significantly perturb Ca^{2+} binding at a site having a Mg^{2+} association constant of <100 M^{-1}. The use of Mg^{2+} concentrations of >5 mM was not possible, due to severe depletion of the radiolabel during the course of the experiment. Even at 5 mM, it was necessary to reduce the number of data points, to keep the loss of $^{45}Ca^{2+}$ from the sample chamber below 10%. It should be noted that an unweighted least-squares treatment of these data, omitting the confidence interval analysis, yielded Mg^{2+} association constants of 11 000 and 74 M^{-1} (*34*).

The binding constant estimates extracted from data collected in K^+-containing buffers (Figure 3D) are perceptibly larger than those measured in Na^+. K_1 increases by approximately one-third, from 2.27×10^7 to 3.05×10^7 M^{-1}. The first Mg^{2+}-binding constant, K_{1M}, shows a similar increase, from 12 300 to 17 300 M^{-1}. The second Ca^{2+}- and Mg^{2+}-binding events display proportionately greater increases in affinity. K_2 increases by a factor of 3.3 in K^+, from 1.05×10^7 to 3.5×10^7 M^{-1}. The best-fit value of K_{2M} is 399, likewise a substantial increase from the poorly determined estimate obtained in Na^+ solution.

ITC. Global least-squares analysis of ITC data offers an alternative to flow dialysis for the estimation of parvalbumin divalent ion affinities. Figure 4 compares select titrations of rat α and β in Na^+- or K^+-containing solution. Panels A−C depict titrations of rat β conducted in Na^+-containing solution, panels D−F titrations of β in K^+, panels G−I titrations of α in Na^+, and panels J−L titrations of α in K^+. The marked variation in the appearance of these thermograms illustrates the wealth of information inherent in these experiments and the rationale for a global ITC-based analytical method.

The rat β system was recently used to demonstrate the utility of this approach (*34*). In that work, samples of the protein—in Na^+-containing buffers—were titrated with Ca^{2+}, with Mg^{2+}, with Ca^{2+} at several fixed levels of Mg^{2+}, with Ca^{2+} in the presence of EDTA, and with Ca^{2+} in the presence of EGTA. The binding constants from that analysis are included in Table 1. Relative to the values determined by flow dialysis, the ITC-derived estimates for K_1 and K_2, 2.45×10^7 and 1.43×10^6 M^{-1}, are slightly larger. The ITC-based method also returns a somewhat smaller value for K_{1M} (9 400 vs 12 300 M^{-1}) and a significantly larger value for K_{2M} (164 M^{-1}).

The results of a comparable analysis in K^+-containing solution are presented herein. It is evident from Figure 4A−F that the solvent cation has a perceptible impact on the divalent ion-binding behavior. From a comparison of panels A and D, it is evident that the enthalpy of the first binding event (occupation of the EF site) is substantially more exothermic in K^+ solution. Panels B and E compare titrations of β with Ca^{2+} in the presence of the competing chelator EGTA, in Na^+ or K^+ solution, respectively. Besides the increased exothermicity of Ca^{2+} binding in K^+ just mentioned, the shapes of the curves differ perceptibly. Whereas the chelator titrates concomitantly with the β EF site in Na^+, the Ca^{2+} affinity of the protein is increased in K^+, to the point that the EF site is occupied preferentially during the initial stage of the titration. Finally, as shown in panels C and F, solvent cation identity has a major effect on the titrations with Mg^{2+}. Binding is far less endothermic in K^+, consistent with a marked increase in Mg^{2+} affinity.

Integrated data for a battery of titrations conducted in the presence of K^+ are displayed in Figure 5. This composite dataset was subjected to nonlinear least-squares minimization. Initial estimates for the Ca^{2+}- and Mg^{2+}-binding enthalpies were obtained from the analysis of single titrations, and the estimates obtained from flow dialysis provided input values for the Ca^{2+}- and Mg^{2+}-binding constants. The solid lines in Figure 5 indicate the best global least-squares fit. The residuals for the various experiments, presented in the lower panels, are largely free of systematic variation. Several of the experiments, however, exhibit anomalies near the equivalence point, for example, the titrations with Ca^{2+} in the presence of EDTA (○) and EGTA (□) shown in Figure 5D. These discrepancies may reflect errors in sample concentration.

The parameter correlation matrix for the system is displayed in Table 2. The correlation coefficients are acceptable, the highest being 0.894. In consequence, the

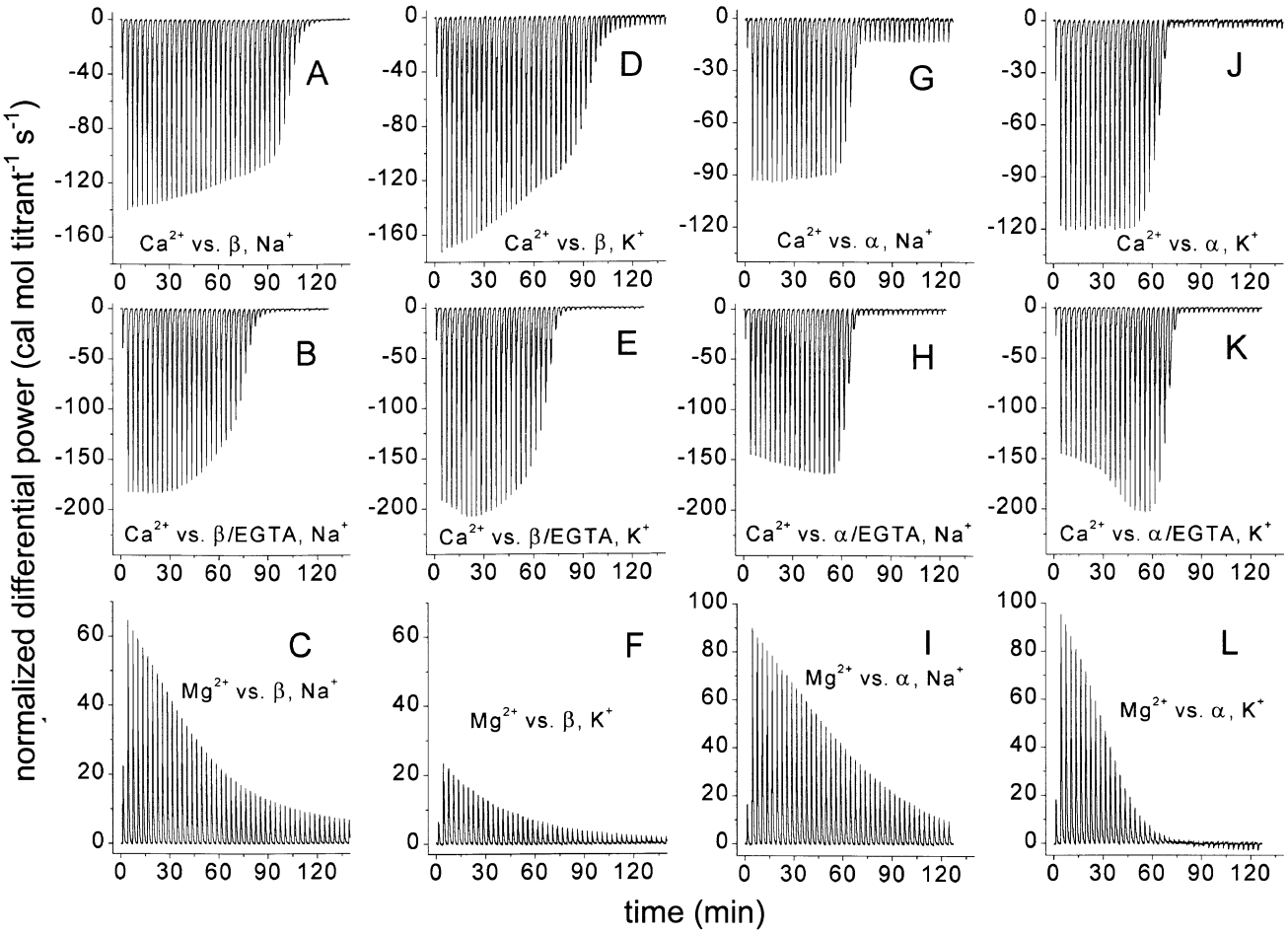

FIGURE 4: Raw ITC data: (A) 4.0 mM Ca^{2+} vs 260 μM β, in Na^+; (B) 2.0 mM Ca^{2+} vs 75 μM β, 0.125 mM EGTA, in Na^+; (C) 5.2 mM Mg^{2+} vs 275 μM β, in Na^+; (D) 1.0 mM Ca^{2+} vs 60 μM β, in K^+; (E) 2.0 mM Ca^{2+} vs 62 μM β, 0.125 mM EGTA, in K^+; (F) 2.0 mM Mg^{2+} vs 60 μM β, in K^+; (G) 1.0 mM Ca^{2+} vs 60 μM α, in Na^+; (H) 2.0 mM Ca^{2+} vs 60 μM α, 0.125 mM EGTA, in Na^+; (I) 2.0 mM Mg^{2+} vs 120 μM α, in Na^+; (J) 2.0 mM Ca^{2+} vs 65 μM α, in K^+; (K) 2.0 mM Ca^{2+} vs 65 μM α, 0.125 mM EGTA, in K^+; (L) 2.0 mM Mg^{2+} vs 65 μM α, in K^+.

parameters are well determined, with narrow confidence intervals. Uncertainties were also examined by Monte Carlo simulation. Briefly, random variations were made to each of the fitting parameters, and a χ^2 value was determined for the resulting parameter set. If the χ^2 value fell below the 68% confidence limit, the parameter values were written to a file. If not, they were discarded. This process was repeated until an arbitrary, large number of parameter sets satisfying the chi-square criterion had been collected. Figure 6 displays the binding constant distributions obtained for the ITC analysis of rat β in K^+ solution.

The optimal parameter values, listed in Table 1, agree well with the estimates from flow dialysis. K_1 is 13% larger (3.45×10^7 vs 3.05×10^7 M^{-1}). The other three binding constants are slightly smaller—3.36×10^6 vs 3.50×10^6 M^{-1} for K_2; 14 000 vs 17 300 for K_{1M}; and 280 vs 399 for K_{2M}. Consistent with the flow-dialysis measurements, the ITC-based method also suggests that the divalent ion affinity of rat β is perceptibly greater in K^+ solution.

Ca^{2+} and Mg^{2+} Affinities of Rat α-Parvalbumin

NMR Spectra of Ca^{2+}-Free Rat α in Na^+ and K^+ Solution. The identity of the major solvent cation strongly influences rat α stability. The T_m for the protein— approximately 46 °C in 0.20 M NaCl, 0.01 M NaP_i, and 0.005 M EDTA—is shifted downward to 35 °C in the corresponding K^+-containing buffer (*26*). The ΔC_p likewise undergoes substantial reduction from 1.4 kcal mol^{-1} K^{-1} in Na^+ solution to 0.53 kcal mol^{-1} K^{-1} in K^+. This latter finding suggests that the protein is less structured in K^+ buffers. The appearance of the ^1H,^{15}N-HSQC spectrum for the Ca^{2+}-free protein lends support to that hypothesis.

The HSQC spectrum collected in 0.15 M KCl and 0.005 M Mes−KOH, pH 6.0, is displayed in Figure 7A; corresponding data collected in Na^+ solution are presented in Figure 7B. A subset of the signals present in the K^+ spectrum appear as doublets, suggesting that at least two conformations of α are populated, with relatively slow rates of interconversion. These doublets are absent in the Na^+ spectrum, and the chemical shift dispersion in the proton dimension appears to be improved. Thus, the binding of Na^+ apparently favors a single, relatively well-structured conformation. In fact, many of the resonances in the latter spectrum exhibit chemical shifts comparable to those observed for the Ca^{2+}-loaded protein (Figure 7C). The behavior of the Gly-56 amide is noteworthy. Whereas it affords an extremely weak signal at 10.38 ppm in K^+ solution, a strong resonance is observed, at 10.88 ppm, in the presence of Na^+. The chemical shift of the Gly-56 amide proton is 10.58 in the Ca^{2+}-bound form.

Flow Dialysis. $^{45}Ca^{2+}$ flow-dialysis data for rat α in both Na^+ and K^+ buffer solutions, at 25 °C, are presented in panels C and D, respectively, of Figure 3. As with β, titrations were

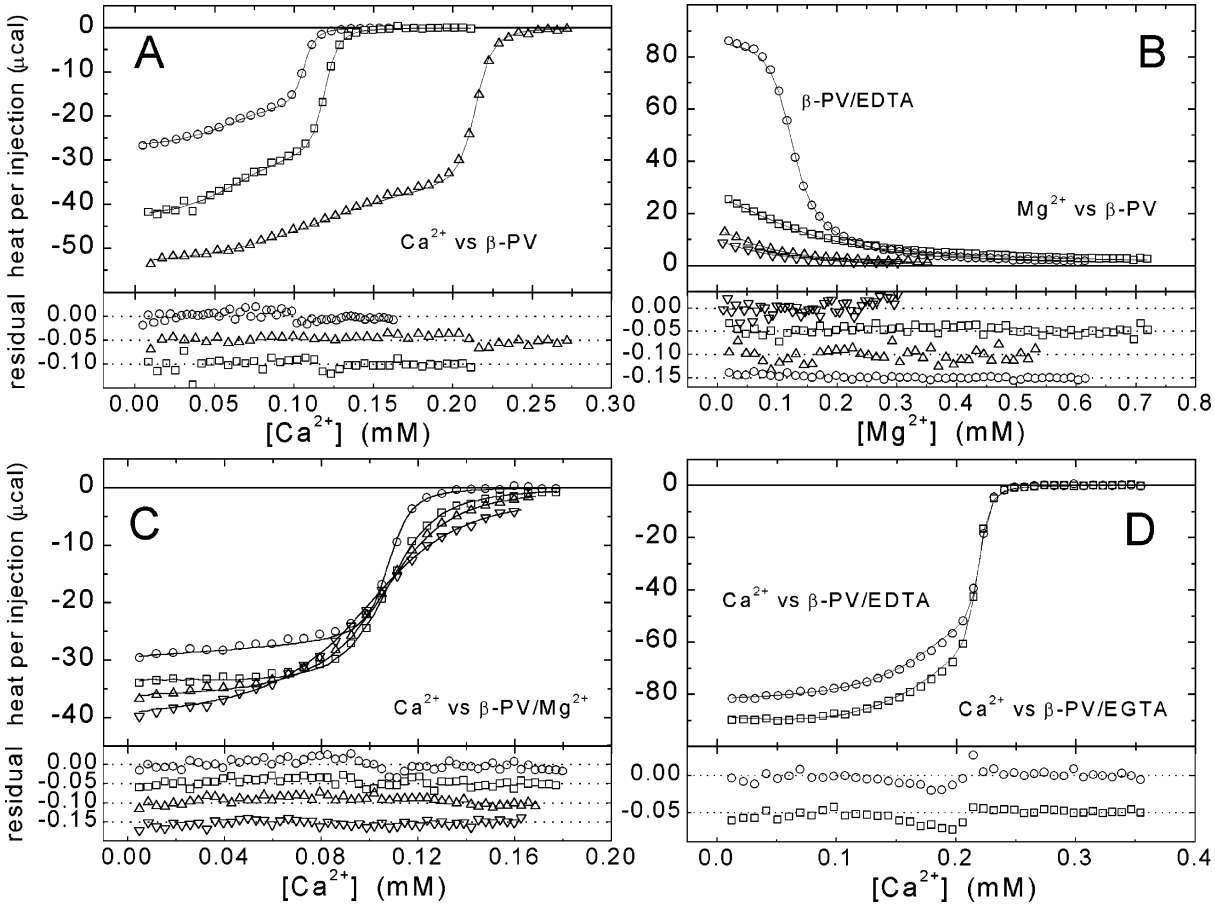

FIGURE 5: ITC analysis of rat β divalent ion-binding behavior in K^+-containing solution: (A) 1.0 mM Ca^{2+} vs 59 μM β-PV (○); 2.0 mM Ca^{2+} vs 62.4 μM β (□); 2.0 mM Ca^{2+} vs 120 μM β (△). (B) 2.0 mM Mg^{2+} vs 58 μM β (▽); 2.0 mM Mg^{2+} vs 63 μM β (△); 4.0 mM Mg^{2+} vs 118 μM β (□); 4.0 mM Mg^{2+} vs 62 μM β, 0.125 mM EDTA (○). (C) 1.0 mM Ca^{2+} vs 60 μM β, 0.50 mM Mg^{2+} (○); 1.0 mM Ca^{2+} vs 60 μM β, 5.0 mM Mg^{2+} (□); 1.0 mM Ca^{2+} vs 60 μM β, 10 mM Mg^{2+} (△); 1.0 mM Ca^{2+} vs 59 μM β, 20 mM Mg^{2+} (▽). (D) 2.0 mM Ca^{2+} vs 63 μM β, 0.125 mM EDTA (○); 2.0 mM Ca^{2+} vs 63 μM β, 0.125 mM EGTA (□).

Table 2: Parameter Correlations for Global Fit of β-PV ITC Data in K^+ Solution at 25 °C

	ΔH_1	ΔH_2	ΔH_{1M}	ΔH_{2M}	k_1	k_2	k_{1M}	k_{2M}
ΔH_1	1.000							
ΔH_2	0.617	1.000						
ΔH_{1M}	0.241	0.232	1.000					
ΔH_{2M}	0.314	0.450	0.487	1.000				
k_1	0.887	0.623	0.352	0.459	1.000			
k_2	0.661	0.846	0.373	0.650	0.816	1.000		
k_{1M}	0.425	0.397	0.418	0.658	0.681	0.716	1.000	
k_{2M}	0.342	0.421	0.419	0.894	0.553	0.732	0.816	1.000

conducted both in the absence of Mg^{2+} (○) and at several fixed levels of the competing ion. Figure 3 emphasizes the disparate Ca^{2+} affinities of the rat α and β isoforms. Whereas the median Ca^{2+} concentration—the concentration producing half-saturation—is 2×10^{-7} M for β in Na^+ solution (Figure 3A) in the absence of Mg^{2+}, the median concentration for α under the same conditions (Figure 3C) is $\sim 10^{-8}$ M. As a result of the latter's much higher affinity for Ca^{2+}, the levels of radioactivity in the eluate early in the titration approach background levels, making flow-dialysis measurements on α challenging. Data from eight separate titrations, conducted in the absence of Mg^{2+} (○), have been superimposed in Figure 3C to provide a qualitative indication of the experimental scatter.

Despite the high affinity of α for Ca^{2+} in Na^+ solution, it is possible to obtain an acceptable least-squares fit to the composite dataset, indicated by the solid lines in Figure 3C.

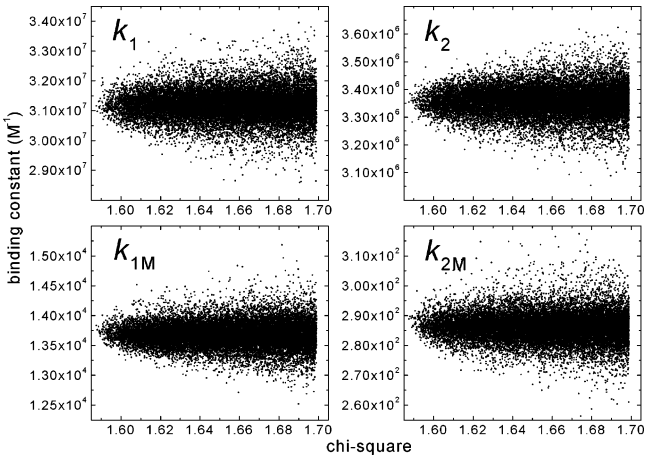

FIGURE 6: Monte Carlo parameter simulations of rat β divalent ion-binding behavior in K^+ solution. The best-fit parameter values from least-squares minimization furnished the starting point for the generation of additional parameter sets satisfying the requirement that $\chi^2 < 1.70$, the value associated with the 68% confidence limit. Each point represents one of 20 000 simulated parameter sets meeting this criterion. The binding constants from each set have been plotted against the associated χ^2 value.

The apparent macroscopic Ca^{2+} constants are 1.74×10^8 and 4.27×10^7 M^{-1}; the corresponding Mg^{2+} values are 3.71×10^4 and 4.97×10^3 M^{-1}.

Although it was apparent that the Ca^{2+} affinity of rat α is higher in K^+-containing solution, we were unable to extract

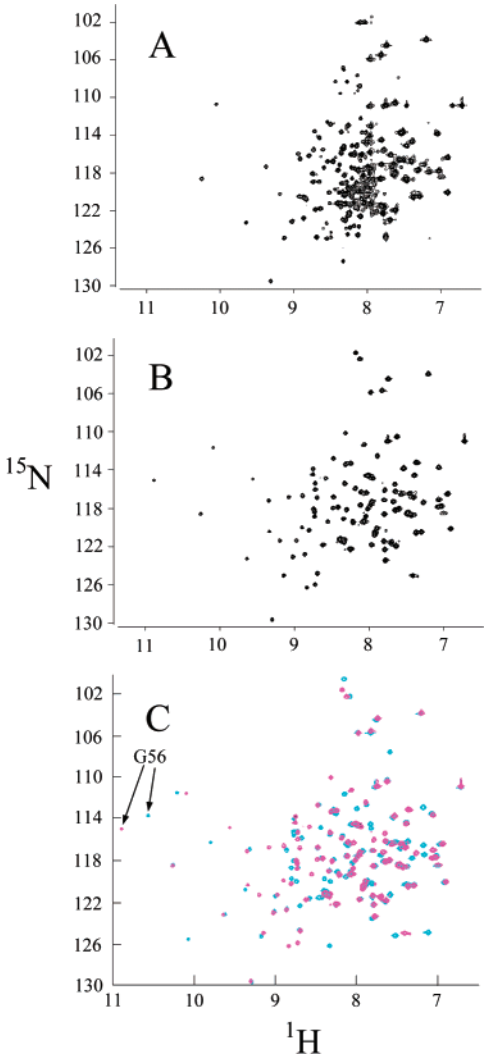

FIGURE 7: ^{1}H,^{15}N-HSQC spectra of rat α: (A) spectrum of 1.0 mM Ca^{2+}-free α, in 0.15 M KCl and 0.005 M Mes-KOH, pH 6.0; (B) spectrum of 1.5 mM Ca^{2+}-free α, in 0.15 M NaCl and 0.005 M Mes−NaOH, pH 6.0; (C) superposition of Ca^{2+}-free α in Na^{+} (magenta) and that of 1.0 mM Ca^{2+}-loaded α (cyan), collected after dialysis against 0.15 M NaCl, 0.005 M Mes−NaOH, pH 6.0, and 0.5 mM Ca^{2+}.

reliable estimates of the Ca^{2+} binding constants by flow dialysis. In the absence of Mg^{2+}, the level of radioactivity in the eluate remains just above background until very late in the titration. As illustrated in Figure 3D, which includes nine separate titrations in the absence of Mg^{2+} (○), uncertainties in the background and sample activities combine to produce an unacceptably high degree of scatter. When this composite dataset was subjected to global nonlinear least-squares minimization, it was not possible to simultaneously accommodate data gathered in the presence and absence of Mg^{2+}.

ITC. Disappointed in our effort to characterize the ion-binding behavior of rat α in K^{+} solution by flow dialysis, we turned to titration calorimetry. As observed for rat *β*, solvent cation identity strongly influences the appearance of the raw ITC data. The normalized thermograms displayed in Figure 4G,J indicate that Ca^{2+}-binding enthalpy is substantially more exothermic in K^{+}. Moreover, when the protein is titrated with Ca^{2+} in the presence of EGTA, binding by the chelator occurs later in the experiment in K^{+} solution (cf. panels H and K of Figure 4)—evidence of the increased Ca^{2+} affinity of the protein. It is also apparent that Mg^{2+} affinity is substantially higher in K^{+} solution. Whereas binding continues throughout the titration in Na^{+} solution (Figure 4I), an apparent endpoint is reached in the presence of K^{+} (Figure 4L).

The divalent ion affinity of α was initially studied by ITC in Na^{+} solution at 25 °C. Integrated data from a battery of 12 separate titrations are displayed in Figure 8. These experiments were simultaneously analyzed by nonlinear least-squares analysis. Initial estimates for the binding enthalpies were obtained from the analysis of single titrations, and the flow-dialysis measurements on α in Na^{+} solution provided starting values for the binding constants. The solid lines through the data points denote the best overall fit to the composite dataset. Residuals for each experiment are plotted in the lower panels. The binding constants obtained by this analysis are slightly larger than those measured by flow dialysis: 2.50×10^{8} and 6.24×10^{7} M^{-1} vs 1.74×10^{8} and 4.27×10^{7} M^{-1} for Ca^{2+}; 3.66×10^{4} and 9.02×10^{3} M^{-1} vs 3.71×10^{4} and 4.97×10^{3} M^{-1} for Mg^{2+}.

From the magnitudes of the binding constants—$K_1 \approx 4K_2$ and $K_{1M} \approx 4K_{2M}$—it is evident that the α CD and EF sites are indistinguishable in Ca^{2+}- or Mg^{2+}-binding assays. The parameter correlation matrix for this system is shown in Table 3. In contrast to the corresponding matrix for rat *β* (Table 2), the enthalpies and binding constants for the two sites are very highly correlated, that is, $R_{ij} \geq 0.98$. This finding, reflecting the functional equivalency of the two sites, indicates that the system could be modeled equally well with an equivalent two-site model.

Attempting to perform the comparable analysis in K^{+} solution at 25 °C, we observed that single titrations of α with Ca^{2+} or Mg^{2+} could not be satisfactorily modeled with an independent two-site model. For Mg^{2+}, the optimal fit yielded $K_1 = 3.0 \times 10^{4}$ and $K_2 = 5.2 \times 10^{4}$ M^{-1} (Figure 9A,B). The magnitudes of the binding constants, $K_1 < 4K_2$, indicate a positive interaction between the two sites. Upon reflection, we concluded that this positive cooperativity might be a consequence of the low conformational stability of rat α in K^{+} solutions (see discussion below). Consistent with this hypothesis, individual titrations at 5 °C were readily accommodated by a non-cooperative two-site model (e.g., Figure 9C,D). The decision was made, therefore, to examine the impact of monovalent cation identity on α divalent ion-binding behavior at 5 °C.

Integrated ITC data gathered in either Hepes-buffered NaCl or Hepes-buffered KCl at 5 °C are displayed in Figures 10 and 11, respectively. The solid lines in each plot indicate the best least-squares fit to the composite dataset. The residuals are displayed below each plot. As for the preceding analyses, parameter uncertainties were evaluated by determining the 68% confidence intervals and performing Monte Carlo simulations of the parameters.

Temperature has a relatively small impact on α divalent ion-binding behavior. The apparent Ca^{2+}-binding constants measured in Na^{+} solution at 5 °C, both ΔH and K values, are essentially identical to those measured at 25 °C. The Mg^{2+} binding constants at the two temperatures differ by only a factor of 2: 1.76×10^{4} and 4.30×10^{3} M^{-1} at 5 °C and 3.66×10^{4} and 9.02×10^{3} M^{-1} at 25 °C. The ratios of K_1/K_2 and likewise K_{1M}/K_{2M} are both ≈4 at 5 °C, implying

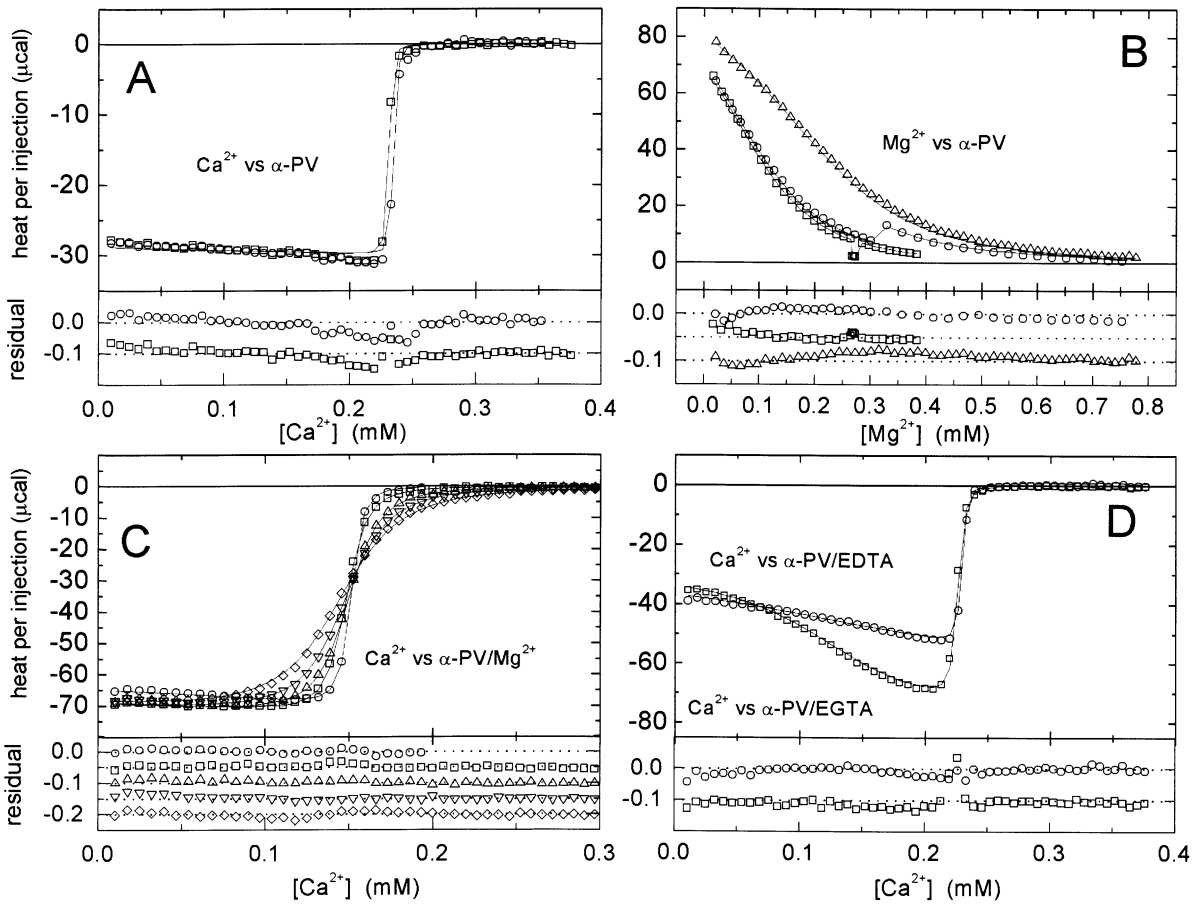

FIGURE 8: ITC analysis of rat α divalent ion-binding behavior in Na^+ solution at 25 °C: (A) 2.1 mM Ca^{2+} vs 130 μM α (○); 2.1 mM Ca^{2+} vs 127 μM α (□); (B) 4.1 mM Mg^{2+} vs 60 μM α (○); 2.0 mM Mg^{2+} vs 57 μM α (□); 4.3 mM Mg^{2+} vs 117 μM α (△). (C) 2.1 mM Ca^{2+} vs 80 μM α, 0.5 mM Mg^{2+} (○); 2.1 mM Ca^{2+} vs 80 μM α, 2.0 mM Mg^{2+} (□); 2.1 mM Ca^{2+} vs 80 μM α, 5.0 mM Mg^{2+} (△); 2.1 mM Ca^{2+} vs 80 μM α, 10 mM Mg^{2+} (▽); 2.1 mM Ca^{2+} vs 80 μM α, 20 mM Mg^{2+} (◇). (D) 2.1 mM Ca^{2+} vs 60 μM α, 0.125 mM EDTA (○); 2.1 mM Ca^{2+} vs 60 μM α, 0.125 mM EGTA (□).

Table 3: Parameter Correlations for Global Analysis of α-PV in Na^+ Solution at 25 °C

	ΔH_1	ΔH_2	ΔH_{1M}	ΔH_{2M}	K_1	K_2	K_{1M}	K_{2M}
ΔH_1	1.000							
ΔH_2	0.997	1.000						
ΔH_{1M}	0.577	0.576	1.000					
ΔH_{2M}	0.587	0.597	0.993	1.000				
K_1	0.886	0.880	0.678	0.687	1.000			
K_2	0.880	0.884	0.682	0.700	0.992	1.000		
K_{1M}	0.589	0.583	0.636	0.654	0.802	0.796	1.000	
K_{2M}	0.588	0.591	0.627	0.658	0.793	0.800	0.992	1.000

that the apparent equivalency of the two sites is retained at the low temperature.

Solvent cation identity has a much greater impact than temperature on divalent ion affinity. Both Ca^{2+}- and Mg^{2+}-binding constants increase by roughly an order of magnitude in K^+ solution. K_1 and K_2 increase from 2.55×10^8 and 6.36×10^7 to 2.94×10^9 and 6.59×10^8 M^{-1}. K_{1M} and K_{2M} increase from 1.76×10^4 and 4.30×10^3 M^{-1} to 2.17×10^5 and 3.71×10^4 M^{-1}. Note that the relative magnitudes of the binding constants differ slightly in K^+—with the K_1/K_2 ratio increasing to 4.5 and K_{1M}/K_{2M} increasing to 5.8. These alterations may indicate that the two sites are not completely equivalent in K^+-containing buffer.

DISCUSSION

It is evident that monovalent cation identity influences parvalbumin divalent ion affinity in an isoform-dependent manner. In the following paragraphs, the results obtained for rat α and β isoforms in Na^+ and K^+ solutions are compared and interpreted in light of the stability data previously reported for the two proteins.

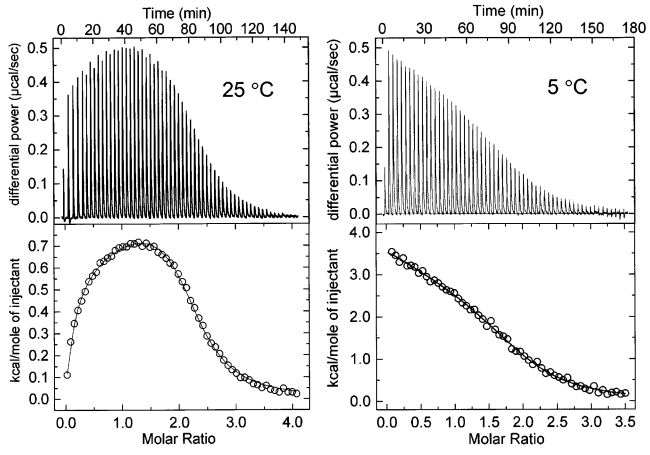

FIGURE 9: Mg^{2+} binding by rat α K^+-containing buffer—effect of temperature: (left) titration of 210 μM rat α with 4.0 mM Mg^{2+}, in 0.15 M KCl and 0.025 M Hepes−KOH, pH 7.4, at 25 °C (raw data are presented in the upper panel, integrated data in the lower panel); (right) 1.0 mM Mg^{2+} vs 60 μM α in K^+ solution at 5 °C (raw and integrated data are presented in the upper and lower panels, respectively).

Impact of Monovalent Ions on Rat β Divalent Ion-Binding Behavior. Although DSC data reported previously indicated

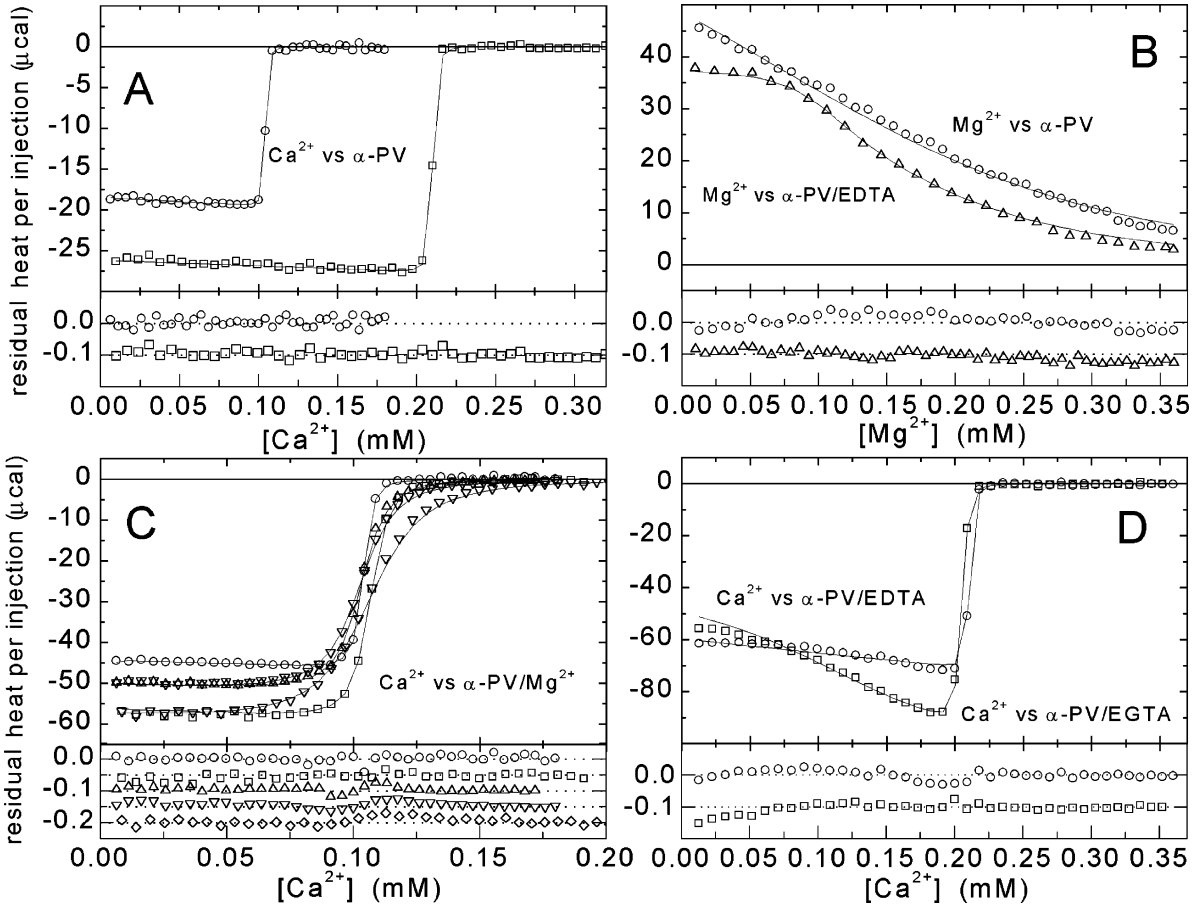

FIGURE 10: ITC analysis of rat α divalent ion-binding behavior in Na^+ solution at 5 °C: (A) 1.0 mM Ca^{2+} vs 57 μM α (○); 2.0 mM Ca^{2+} vs 115 μM α (□). (B) 2.0 mM Mg^{2+} vs 115 μM α (○); 2.0 mM Mg^{2+} vs 57 μM α, 0.110 mM EDTA (△). (C) 1.0 mM Ca^{2+} vs 57 μM α, 0.50 mM Mg^{2+} (○); 2.0 mM Ca^{2+} vs 55 μM α, 2.0 mM Mg^{2+} (□); 1.0 mM Ca^{2+} vs 56 μM α, 5.0 mM Mg^{2+} (△); 1.0 mM Ca^{2+} vs 56 μM α, 10 mM Mg^{2+} (▽); 2.0 mM Ca^{2+} vs 55 μM α, 20 mM Mg^{2+} (◇). (D) 2.0 mM Ca^{2+} vs 56 μM α, 0.12 mM EDTA (○); 2.0 mM Ca^{2+} vs 56 μM α, 0.10 mM EGTA (□).

that β binds either Na^+ or K^+, the apparent binding capacities differ for the two ions. Whereas the estimated stoichiometry for Na^+ binding is 1.8 ± 0.2 equiv in 0.24 M Na^+, the stoichiometry of K^+ binding is just 1.1 ± 0.2 equiv at the same ionic strength. Titration of the protein with Na^+ at low ionic strength (1 mM imidazole−EDTA, pH 7.4) produced exothermic heat effects well in excess of those produced by titration of buffer alone. Analysis of these data, assuming two identical sites, yielded estimates for the apparent binding constant and average enthalpy of binding of 60 M^{-1} and −4.9 kcal/mol, respectively. In anticipation of the subsequent discussion, it should be noted that there is no evidence that the monovalent ion-binding sites are in fact equivalent. However, there was insufficient information in the dataset to uniquely fit more complex models. Titration with K^+ in 1 mM imidazole−EDTA, pH 7.4, yielded apparent binding constant and enthalpy values of 55 M^{-1} and −8.8 kcal/mol, respectively. In both cases, inclusion of 100 μM Ca^{2+} abolished the binding events, suggesting that the bound cations occupy the EF-hand motifs.

In contrast to more typical parvalbumin isoforms, the two EF-hand motifs in rat β are distinctly nonequivalent—the EF site exhibiting substantially greater affinity for divalent ions. Resultingly, the sites are occupied sequentially during titrations with Ca^{2+} or Mg^{2+}, with the microscopic association constants, k_1 and k_2, corresponding to the binding constants for the EF and CD sites, respectively.

ITC and flow-dialysis studies both indicate that the divalent ion affinities of both sites are modestly higher when measured in K^+ solution. The Ca^{2+} affinities determined by ITC for the EF and CD sites are increased by factors of 1.41 and 2.35, respectively, producing an overall $\Delta\Delta G°'$ for Ca^{2+} binding of −0.7 kcal/mol (Table 4). The ITC-measured Mg^{2+}-binding constants increase by 1.48 and 1.71, respectively, yielding a $\Delta\Delta G$ value of roughly −0.6 kcal/mol.

K^+ Binds at the β CD Site. Although both EF-hand motifs in rat β bind Na^+, only one binds K^+. The previous suggestion that the lone K^+ is bound in the CD loop (*26*) was based on the lanthanide ion-binding studies by Sykes and co-workers. Whereas the typical parvalbumin EF site displays little size discrimination, the CD site displays a preference for larger ions (*40*, *41*), and the rat β CD site exhibits a particularly strong preference for the larger lanthanides (*42*). Reasoning that this preference might extend to monovalent ions, we suggested that the larger K^+ binds to the CD site (*26*).

The enthalpy changes for Ca^{2+} binding reported here support that assignment. If the CD site can accommodate either Na^+ or K^+, then Ca^{2+} binding will entail obligatory monovalent ion dissociation, regardless of the solvent system. Accordingly, ΔH_2 for Ca^{2+} binding should be largely independent of cation identity, as observed (−3.43 kcal/mol in K^+ vs −3.46 kcal/mol in Na^+). On the other hand, if the EF site binds only Na^+, then the Ca^{2+}-binding event will

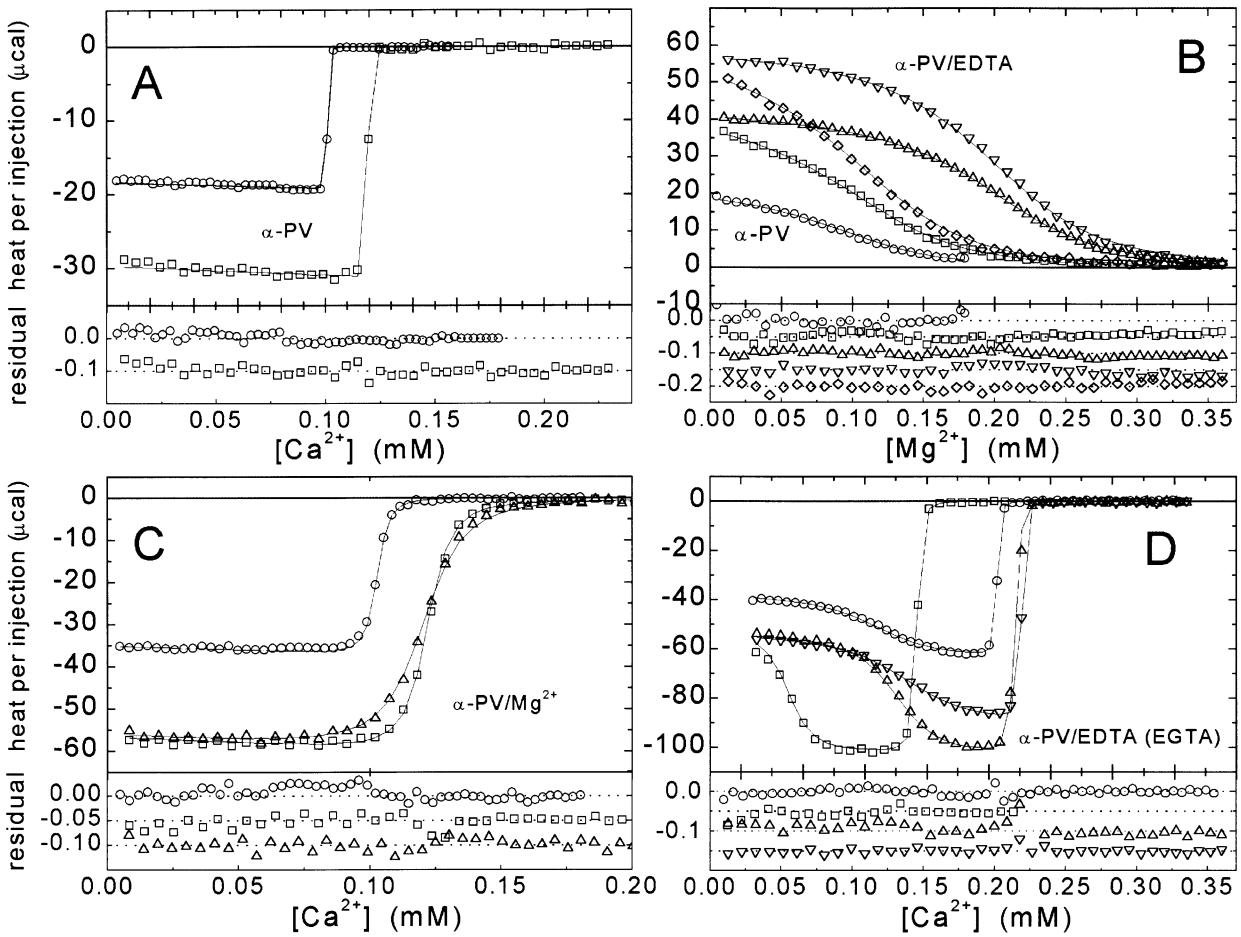

FIGURE 11: ITC analysis of rat α divalent ion-binding behavior in K^+ solution at 5 °C: (A) 0.95 mM Ca^{2+} vs 56 μM α (○); 1.93 mM Ca^{2+} vs 65 μM α (□). (B) 1.0 mM Mg^{2+} vs 64 μM α (○); 2.0 mM Mg^{2+} vs 65 μM α (□); 2.0 mM Mg^{2+} vs 64 μM α (◇); 2.0 mM Mg^{2+} vs 62 μM α, 0.12 mM EDTA (△); 2.0 mM Mg^{2+} vs 64 μM α, 0.12 mM EDTA (▽). (C) 1.0 mM Ca^{2+} vs 95 μM α, 1.0 mM Mg^{2+} (□); 2.0 mM Ca^{2+} vs 64 μM α, 3.0 mM Mg^{2+} (○); 2.0 mM Mg^{2+} vs 95 μM α, 10 mM Mg^{2+} (△). (D) 2.0 mM Ca^{2+} vs 64 μM α, 0.12 mM EDTA (▽); 2.0 mM Ca^{2+} vs 51 μM α, 0.12 mM EDTA (○); 2.0 mM Ca^{2+} vs 19 μM α, 0.095 mM EGTA (□); 2.0 mM Ca^{2+} vs 64 μM α, 0.115 mM EGTA (△).

Table 4: Summary of Divalent Ion-Binding Energetics[a]

protein	cation	T (°C)	Ca^{2+} binding ΔG_{total}[b]	ΔH_{total}	$-T\Delta S_{total}$	Mg^{2+} binding ΔG_{total}[b]	ΔH_{total}	$-T\Delta S_{total}$
β-PV	Na^+	25	−18.4	−7.6	−10.8	−8.4	7.2	−15.6
	K^+	25	−19.1	−8.9	−10.2	−9.0	7.2	−16.1
α-PV	Na^+	25	−22.0	−5.6	−16.4	−11.6	8.2	−19.7
	Na^+	5	−20.6	−5.5	−15.1	−10.0	9.4	−19.4
	K^+	5	−23.2	−7.9	−15.3	−12.6	6.7	−19.3

[a] All energies reported as kcal/mol. [b] Calculated with the expression $\Delta G = -RT \ln K_2K_1$, using the macroscopic binding constants listed in Table 1.

differ fundamentally in the two solvent systems. In Na^+ solution, Ca^{2+} binding will require monovalent ion dissociation. In K^+ solution, however, Ca^{2+} binds to a vacant site. Because there is no requirement for (endothermic) monovalent ion release in the latter case, the ΔH_1 for Ca^{2+} binding should be more exothermic, as observed (−5.5 kcal/mol in K^+; −4.1 kcal/mol in Na^+).

Rat α. DSC studies indicated that the α isoform binds 1.1 ± 0.1 equiv of Na^+ but has very low affinity for K^+. Consistent with these findings, titration of α with Na^+ in 1 mM imidazole−EDTA, pH 7.4, produces large exothermic heat effects, whereas titration with K^+ under comparable conditions produces heat effects identical to those resulting from titration of buffer alone (*26*). Least-squares analysis of the Na^+ titration data, assuming a stoichiometry of 1.0, yielded an apparent binding constant of 120 M^{-1}. As with β, Na^+ binding was abolished in the presence of Ca^{2+}, implying that the monovalent ion occupies one of the EF-hand motifs.

The observation that rat α divalent ion affinity is much higher in K^+ solution than in Na^+ solution is additional evidence for the competitive nature of the monovalent ion binding. In fact, the Ca^{2+} affinity in K^+ solution proved to be too high to accurately measure by flow dialysis, providing the incentive for development of an ITC-based analytical scheme.

The latter method worked well at 25 °C in Na^+-containing buffer, yielding apparent binding constants in good agreement with those obtained by flow dialysis. However, it was not possible to obtain a satisfactory fit with a simple two-site model to ITC data gathered in K^+ at the same temperature. The reason became evident upon close inspection of individual titrations. Whereas titrations with Ca^{2+} in the presence of Mg^{2+} were amenable to treatment with an independent two-site model, the binding constants obtained from analysis of single titrations with Ca^{2+} or Mg^{2+} indicated substantial positive cooperativity.

Upon reflection, it was concluded that this behavior derived from the marginal stability of rat α in K^+ solution. In 0.12 M KCl, 0.010 M KP_i, and 0.005 M KEDTA, pH 7.4, the apparent standard free energy change for denaturation at 25 °C is just +1.13 kcal/mol (*26*). Thus, ~13% of the protein is unfolded under these conditions. For this population of molecules, Ca^{2+} binding is linked to folding. Besides contributing an additional enthalpic component to the divalent ion-binding reaction, the refolding phenomenon that accompanies the first binding event facilitates the second event.

This behavior is not observed in Na^+ solution at 25 °C because the binding of Na^+ significantly stabilizes the folded form of the apoprotein. For example, the T_m increases from 35.3 °C in 0.20 mM KCl, 0.01 M KP_i, and 0.005 M KEDTA, pH 7.4, to 45.8 °C in 0.20 M NaCl, 0.01 M NaP_i, and 0.005 M NaEDTA (*26*). The ΔC_p for denaturation also increases from 0.53 kcal mol^{-1} K^{-1} in K^+ solution to 1.4 kcal mol^{-1} K^{-1} in Na^+ solution. The latter finding suggests that the Ca^{2+}-free form of rat α is more completely folded in Na^+, exposing substantially less apolar surface area. The conformational stability of Ca^{2+}-free α, estimated at 1.1 kcal/mol in 0.15 M KCl at 25 °C, increases to 3.0 kcal/mol in 0.15 M NaCl. Under the latter conditions, <1% of the protein is unfolded.

The analysis of rat α divalent ion-binding behavior was ultimately conducted at 5 °C. At this temperature, the estimated stability of the protein is increased to 2.9 kcal/mol, eliminating problems associated with protein instability. Comparison of the ITC analyses conducted in Na^+ at 5 and 25 °C indicates that the shift in temperature has a fairly modest effect on the free energy changes associated with divalent ion binding. The apparent Ca^{2+}-binding constants are essentially unchanged, and the Mg^{2+} constants decrease by a factor of only 2.

In contrast to rat *β*, the CD and EF sites in rat α behave indistinguishably in titrations with Ca^{2+} and Mg^{2+}. In Na^+-containing solution at 5 °C, the macroscopic Ca^{2+}-binding constants are 2.55×10^8 and 6.36×10^7 M^{-1}, respectively. The corresponding Mg^{2+} values are 1.76×10^4 and 4.30×10^3 M^{-1}. Both pairs of constants differ by a factor of 4, indicating that the two sites have apparently identical divalent ion affinities.

Because α binds a single equivalent of Na^+, one might predict that the switch to K^+ solution would primarily affect divalent ion affinity at just one of the two sites. Instead, the affinities of both sites increase by comparable factors. The macroscopic Ca^{2+}-binding constants are 2.94×10^9 and 6.59×10^8 M^{-1}. The ratio of K_1 to K_2 is 4.5, implying that the apparent equivalence of the binding sites is largely maintained in the presence of K^+. The corresponding Mg^{2+} values are 2.17×10^5 and 3.71×10^4 M^{-1}, for a ratio of 5.8, suggesting perhaps that the sites may not be exactly equivalent with respect to Mg^{2+} binding. There is NMR and X-ray crystallographic evidence that Ca^{2+} and Mg^{2+} do not provoke precisely the same conformational alterations upon binding (*43*, *44*).

Thus, rat α divalent ion affinity is substantially higher in K^+ solution. In Na^+-containing buffers at 5 °C, the apparent ΔG values for Ca^{2+} and Mg^{2+} binding are −20.6 and −10.0 kcal/mol, respectively (Table 4). In K^+ solution, these values shift to −23.2 and −12.6 kcal/mol, respectively. The ITC data suggest that the more favorable free energies of binding

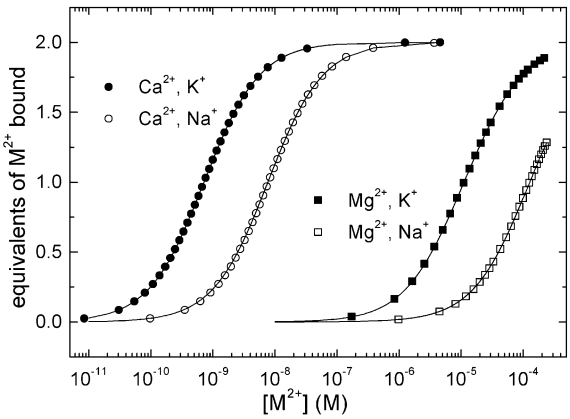

FIGURE 12: Monte Carlo simulation of rat α divalent ion-binding behavior, with explicit consideration of monovalent cation binding: Ca^{2+}-binding data, in Na^+ (○) or K^+ (●); Mg^{2+}-binding data, in Na^+ (□) or K^+ (■). Solid lines indicate the best fit to the data.

in K^+ reflect enthalpic gains. The overall enthalpy change for Ca^{2+} binding shifts from −5.5 kcal/mol in Na^+ to −7.9 kcal/mol in K^+, a $\Delta\Delta H$ of −2.4 kcal/mol. Because the $\Delta\Delta G$ value is −2.6 kcal/mol, the entropic contribution to the binding free energy change ($-T\Delta\Delta S$) is just −0.2 kcal/mol. For Mg^{2+}, the overall ΔH shifts from an estimated 9.4 kcal/mol in Na^+-containing buffer to 6.7 kcal/mol in K^+, a $\Delta\Delta H^{\circ\prime}$ of −2.7 kcal/mol. Given the $\Delta\Delta G_{Mg}$ value of −2.6 kcal/mol, $-T\Delta\Delta S$ must equal 0.1 kcal/mol, slightly unfavorable.

The more favorable divalent ion-binding enthalpy in the presence of K^+ is consistent with other data on the protein. For example, DSC analyses indicate that rat α is less tightly folded in K^+ (*26*). Whereas the ΔC_p for denaturation is 1.4 kcal mol^{-1} K^{-1} in Na^+, it is just 0.53 kcal mol^{-1} K^{-1} in K^+. Moreover, the appearance of the NMR spectrum (Figure 7B,C) likewise suggests that rat α is less structured in K^+ solution. Binding of divalent ions to this relatively unstructured state of the protein would provoke substantial folding, and the concomitant increase in non-covalent interactions would be manifested in more exothermic binding.

Because the binding models used to fit the rat α flow dialysis and ITC data in Na^+ solution did not explicitly consider competition by Na^+, the measured binding constants are apparent values. In contrast, the Ca^{2+}- and Mg^{2+}-binding constants measured for α in K^+ represent "true" binding constants, that is, unperturbed by monovalent ion competition. We eventually recognized that divalent ion-binding data obtained for rat α in Na^+ and K^+ could be analyzed simultaneously to extract an estimate for the Na^+ affinity.

Monte Carlo simulations were conducted as described under Materials and Methods. Binding curves were extracted from four relevant ITC experiments: titrations with Ca^{2+} in either Na^+ or K^+ and titrations with Mg^{2+} in either Na^+ or K^+ (Figure 12). These data were then simulated with the model described by eqs 6 and 7, to obtain estimates for K_{01} and K_{11}, the constants for binding of Na^+ to the apo- and singly Ca^{2+}-bound species. The values thus determined were 640 and 50 M^{-1}. The former is substantially larger than the value determined by direct titration of the protein with Na^+. Conceivably, the conformational change provoked by Na^+ binding is more favorable at physiological ionic strength than in the 1 mM imidazole−EDTA solution employed for the direct titration.

Divalent Ion Binding by α Is Cooperative. Whether the assays are conducted in K^+ or Na^+ solution, Ca^{2+} ion binding by rat α is macroscopically noncooperative, that is, $K_1 \approx 4K_2$, implying that the CD and EF sites are functionally equivalent. However, only one of the two, tentatively identified as the CD site by NMR data (see below), binds Na^+. Moreover, although Na^+ is bound at just one site, the divalent ion affinities of both sites decrease in parallel in the presence of Na^+.

Macroscopic binding studies are of limited utility for detecting and characterizing cooperative binding phenomena (*45*). For a cooperative system, if k_1 and k_2 are the intrinsic Ca^{2+}-binding constants for the two parvalbumin sites, the two macroscopic constants, K_1 and K_2, are equal to

$$K_1 = k_1 + k_2; \quad K_2 = c_{12}k_2k_1/K_1 \tag{10}$$

where c_{12} is a cooperativity coefficient. Equation 10 is a restatement of eq 3, allowing for a positively cooperative interaction between the sites. If ρ is equal to k_2/k_1, macroscopic positive cooperativity requires that

$$4c_{12}\rho - (1 + \rho)^2 > 0 \tag{11}$$

In essence, the two sites must have comparable intrinsic ligand affinities in order to reveal macroscopic positive cooperativity. If k_1 is substantially larger than k_2, binding can appear to be noncooperative, or negatively cooperative, even though $c_{12} > 1$.

The Ca^{2+}-binding data for rat α can be accommodated equally well with site-specific binding constants, employing a model that includes positively cooperative divalent ion binding and Na^+ binding at a specific site (see Materials and Methods, eqs 8 and 9). The best fit—indistinguishable from that shown in Figure 12A—is obtained with $k_1 = 2.68 \times 10^9$, $k_2 = 2.32 \times 10^8$, $c_{12} = 3.12$, and $k_{Na} = 630\ M^{-1}$. This result suggests that the two sites in the α isoform have decidedly different intrinsic Ca^{2+} affinities but are rendered functionally equivalent by a positively cooperative interaction between them.

Alternatively, the presence of Na^+ at the CD site could antagonize Ca^{2+} binding at the EF site. Because this explanation would require the competing monovalent ion to have a similar impact on the local and remote sites, it seems less likely. However, some combination of the two phenomena could also produce the observed attenuation of the EF site affinity in the presence of Na^+. It is worth emphasizing that both explanations require a substantial conformationally mediated interaction between the two EF-hand motifs.

Putative Identity of the Na^+-Binding Site in Rat α. The ^1H,^{15}N-HSQC spectrum of Ca^{2+}-free rat α was acquired in Na^+ solution and in K^+ solution. The spectrum collected in the presence of Na^+ bears surprising similarity to that of the Ca^{2+}-bound protein (Figure 7B,C). Many of the resonances are superimposable in the two spectra, or nearly so. The behavior of the G56 resonance is particularly noteworthy. The G56 amide proton yields the most strongly deshielded ^1H signal in the spectrum of the Ca^{2+}-loaded protein (10.58 ppm). In the spectrum of the Ca^{2+}-free protein collected in Na^+ solution, it is likewise the most downfield resonance, with a chemical shift of 10.88. In K^+, by contrast, G56 produces an extremely weak signal near 10.34 ppm (Figure 7A). If the chemical shift of G56 is an indicator of CD site occupation, it is likely that the lone Na^+ resides in the CD site.

It is interesting that the Na^+ binding event—and the concomitant neutralization of a single charge—has such a major effect on the conformational equilibrium of the protein. Although we previously speculated that the Na^+ is bound in the EF site (*26*), the substantial structural consequences attendant to the binding event are perhaps more consistent with binding in the CD pocket. Whereas the EF site is positioned proximal to the C terminus, the CD site is positioned near the center of the primary sequence. It is more likely that overall protein conformation would be more sensitive to the occupational state of the CD site than to that of the EF site.

Relative Energetics of Divalent Ion Binding by Rat α and β. Because of their distinct monovalent ion-binding properties, the perceived difference between rat α and β with respect to divalent ion-binding behavior depends on solvent cation identity. The overall apparent standard free energies for Ca^{2+} and Mg^{2+} binding by rat α and β are listed in Table 4. When the assays are conducted in Na^+-containing solution, the apparent standard free energies for Ca^{2+} and Mg^{2+} binding are 3.6 and 3.2 kcal/mol, respectively, more favorable for α. However, inspection of the α binding data collected at 5 °C reveals that the free energies of Ca^{2+} and Mg^{2+} binding for α are both 2.6 kcal/mol more favorable in K^+ than in Na^+. Thus, in K^+ solution, the free energies of Ca^{2+} and Mg^{2+} binding are predicted to be 6.2 and 5.8 kcal/mol, respectively, more favorable for α than for β.

The disparate behaviors of the α and β EF sites in K^+ solution deserve comment. The affinity of the α site, obtained from Monte Carlo simulation with site-specific binding constants, is $2.3 \times 10^8\ M^{-1}$. The corresponding value for the β site is $3.1 \times 10^7\ M^{-1}$, calculated from the macroscopic values in Table 1, using eq 4. Thus, the affinity of the α EF site for Ca^{2+} is nearly an order of magnitude higher than that of the β site. Ca^{2+} binding at the EF site in β could conceivably be antagonized by the presence of K^+ at the CD site; that is, the conformation of the K^+-bound CD site may not be optimal for binding of Ca^{2+} at the EF site. Alternatively, the affinity of the β EF site may be inherently lower in β. In this context, ^{15}N NMR relaxation studies from this laboratory indicated that the order parameters for the residues in the AB and D/E regions of the rat β molecule are higher in the Ca^{2+}-free state than in the Ca^{2+}-bound state (*46*). This finding was interpreted as evidence that a portion of the rat β Ca^{2+}-binding energy is used to pay for a conformational change involving the AB and D/E regions.

To distinguish between these two possibilities, it will be necessary to conduct divalent ion-binding studies on rat β under solution conditions in which the CD site is not occupied by monovalent cations. The fact that the CD site divalent ion affinity is higher in K^+ solution suggests that K^+ is bound somewhat less tightly than Na^+. If so, then monovalent ion binding might be abolished in the presence of a still larger alkali metal ion, for example, Rb^+ or Cs^+. Alternatively, replacement of the alkali metal by either tetramethylammonium or imidazolium cation may eliminate monovalent cation binding by the CD site.

Comparison with Previous Work. Published values of rat α divalent ion affinity in K^+ solution show considerable

variation. Pauls et al. (*17*) reported an average intrinsic association constant of 2.4×10^7 M^{-1}, measured in 0.15 M KCl and 50 mM Tris-HCl, pH 7.5. In contrast, Rinaldi et al. (*19*) reported intrinsic Ca^{2+} association constants of 8.3×10^8 and 5.3×10^8 M^{-1}, determined in 0.15 M KCl and 0.025 M Hepes, pH 7.5. Flow dialysis was employed in both cases, and residual Ca^{2+} was removed in both cases by precipitation with trichloroacetic acid (*47*). Using the fluorescent Ca^{2+} indicator, fluo-3, Eberhard and Erne (*18*) measured an average association constant of 1.5×10^8 M^{-1} at 25 °C, in 0.15 M KCl and 0.020 M Hepes−KOH, pH 7.2. More recently, Thépault et al. (*48*) reported an average Ca^{2+} association constant of 2×10^8 M^{-1}, although the data and experimental conditions were not described.

Although the impact of monovalent ions on parvalbumin divalent ion affinity has received relatively little attention, Eberhard and Erne (*18*) have measured the divalent ion affinity of rat α in Na^+- and K^+-containing buffers. They likewise observed higher divalent ion affinity in the presence of K^+. However, their binding constant estimates are nearly an order of magnitude smaller than those reported here. In addition, the values that they measured in K^+ differed from those measured in Na^+ by just a factor of 4, rather than the order of magnitude that we observe. Moreover, whereas calorimetric measurements unequivocally show the binding of Mg^{2+} to be endothermic, their binding data—collected as a function of temperature—suggest that the binding of Mg^{2+} is slightly exothermic.

Conceivably, the method used by Eberhard and Erne to remove residual Ca^{2+}—a 30 min exposure to 4 M urea at room temperature, in the presence of EDTA-derivatized polyacrylamide—may have resulted in modification of the protein. As the data presented in Figure 2 clearly illustrate, rat α is susceptible to modification in the Ca^{2+}-free state, and the oxidized protein exhibits attenuated affinity for Ca^{2+}. Denaturing levels of urea may heighten this susceptibility and/or facilitate other undesirable reactions (e.g., reaction of lysyl side chains with cyanate impurities).

Physiological Significance of Monovalent Ion Binding. Parvalbumin monovalent ion-binding behavior may have physiological relevance. Although K^+ is the major intracellular solvent cation, the intracellular sodium concentration ($[Na^+]_i$) is not negligible. As a rule of thumb, intracellular Na^+ levels vary from 10 to 50 mM, depending on cell type. For example, $[Na^+]_i$ is 29 ± 5 mM in mouse hepatocytes (*49*), 7.8 ± 3.3 mM in kidney proximal tubule cells (*50*), 8.9 ± 3.8 mM in rat brain neurons (*51*), and 7.2 ± 0.5 mM in rat skeletal muscle (*52*).

Importantly, intracellular Na^+ levels can fluctuate in response to physiological and pathological events. In excitable cells, action potentials can produce significant increases in $[Na^+]_i$. For example, a chain of 20 action potentials produced transient 4 mM increases in $[Na^+]_i$ CA1 pyramidal neurons in hippocampal slices (*53*). Spontaneous, transient increases in $[Na^+]_i$ of 5 mM were also observed in cultured hippocampal neurons (*51*). Artificial hyperpolarization of dopamine-sensitive neurons, meant to mimic the effect of dopamine exposure, produced significant increases in $[Na^+]_i$ (*54*). Ischemia can produce much larger changes. In one study on isolated rat CA1 neurons, a 3−4 min period of anoxia caused a 27 mM increase in $[Na^+]_i$ (*55*). In a study on rat hippocampal slices, 10 min of hypoxia increased $[Na^+]_i$ by 218% (*56*). In another study on rat hippocampal slices, hypoxia produced a $\Delta[Na^+]_i$ of 24 ± 8 mM (*57*). Given a Na^+-binding constant of 650 M^{-1}, changes of this magnitude would significantly attenuate rat α Ca^{2+} and Mg^{2+} affinities and, presumably, affect the ability of parvalbumin to buffer cytosolic Ca^{2+} levels.

The physiological significance, if any, of monovalent ion binding by β is less obvious. Expression of the protein in postnatal mammals is apparently restricted to the outer hair cells (OHCs) of the mammalian auditory organ (*15*, *16*), where its concentration is estimated at 0.5 mM (*58*). The composition of the extracellular fluid (endolymph) bathing the apical surface of the OHC is unique—high in K^+ (157 mM) and low in Na^+ (1 mM) and Ca^{2+} (20 μM) (*59*). As a consequence, the OHCs experience a large, continuous K^+ flux through relatively nonselective transduction channels. Modulation of this standing current by mechanoacoustic vibration of the auditory organ causes these cells to undergo audio frequency cycles of contraction and elongation (*60*, *61*). This phenomenon, termed electromotility, results from voltage-dependent conformational changes in prestin, a highly abundant protein in the OHC lateral membrane (*62*). The mechanical disturbances produced by electromotility are believed to amplify the original acoustic signal. Conceivably, the recruitment of the β isoform to the OHC is related to its ability to bind K^+. It should be noted that the nearby inner hair cell (IHC), likewise bathed by endolymph, expresses the α isoform exclusively (*14*). However, the K^+ flux through the inner hair cell is much lower than that in the outer hair cell.

CONCLUSIONS

The potential impact of solvent cations on parvalbumin divalent ion-binding behavior has been largely neglected. It is evident, however, that monovalent cations can modulate parvalbumin divalent ion affinity and that they do so in an isoform-dependent manner. Rat α exhibits substantial affinity for Na^+, but not K^+, and competition by Na^+ significantly attenuates divalent ion affinity. NMR data suggest that the lone Na^+ ion is bound in the CD ion-binding loop. Simultaneous analysis of divalent ion-binding data in K^+ and Na^+ yields an estimate of 1.5 mM for the Na^+ dissociation constant. The analysis also suggests that divalent ion binding is positively cooperative, even though the macroscopic binding data can be modeled with the assumption of two equivalent sites. The attenuation of Ca^{2+} and Mg^{2+} affinity by Na^+ may have physiological relevance.

Rat β can bind either Na^+ or K^+. Previous work indicated that the binding capacity for Na^+ approaches 2 equiv, consistent with binding at both the CD and EF sites. By contrast, the protein binds a single equivalent of K^+. Whereas the apparent Ca^{2+}-binding enthalpy for the EF site is substantially larger in K^+ solution, the CD site enthalpy is unchanged, suggesting that the lone K^+ ion is bound at the CD site. Although the affinity of the vacant β EF site is much lower in K^+ solution than the corresponding site in α, it is not presently known whether this disparity reflects an intrinsic difference between the two proteins or whether the EF site affinity is antagonized by the presence of K^+ at the β CD site.

The physical basis for the disparate monovalent cation-binding behavior of rat α and β is presently conjectural. The

two proteins differ substantially in net charge. Whereas α has a predicted net charge of −5, β has a predicted charge of −15. Thus, the greater charge on β might provide the driving force for binding of a second equivalent of Na^+ to the apoprotein. Alternatively, the disparate monovalent ion-binding properties may reflect the difference in conformational stability. Ca^{2+}-free β is substantially more stable than α, due to the presence of Pro-21 and Pro-26 (*25*). As a result, the EF site in Ca^{2+}-free β may be more structured than that in Ca^{2+}-free α, so that Na^+ binding to the β EF site would carry a smaller entropic penalty.

Although the exclusive binding of K^+ by β is presumably related to the preference of the β CD site for larger cations, the basis for that preference is uncertain. Significantly, the virtually invariant PV sequence triad, F57−I58−E59, is replaced by Y57−L58−D59 in the mammalian β isoform. These substitutions could potentially expand the CD binding pocket. For example, the requirement for solvent exposure of the Tyr-57 hydroxyl may produce an outward movement of the CD binding loop. Moreover, residue 58 plays a dual structural role—the side chain serving to anchor the CD site to the protein core and the amide and carbonyl groups contributing to the segment of antiparallel β structure linking the CD and EF sites. Replacement of isoleucine by leucine at this position could subtly alter the path of the peptide chain. Finally, Asp-59 allows the binding loop substantially greater freedom than does Glu-59, which, by directly coordinating the bound divalent ion, effectively immobilizes the peptide backbone.

REFERENCES

1. Berridge, M. J. (1993) Inositol trisphosphate and calcium signaling, *Nature 361*, 314−325.
2. Berridge, M. J. (1997) Elementary and global aspects of calcium signaling, *J. Physiol. 499*, 291−306.
3. Kretsinger, R. H. (1980) Structure and evolution of calcium modulated proteins, *CRC Crit. Rev. Biochem. 8*, 115−164.
4. Kawasaki, H., and Kretsinger, R. H. (1994) Calcium-binding proteins 1: EF-hands, *Protein Profile 1*, 343−517.
5. Celio, M. R., Pauls, T., and Schwaller, B. (1996) in *Guidebook to the Calcium-Binding Proteins*, Oxford University Press, New York.
6. Seamon, K. B., and Kretsinger, R. H. (1983) Calcium-modulated proteins, in *Calcium in Biology* (Spiro, T. G., Ed.), pp 3−51, Wiley, New York.
7. Wnuk, W., Cox, J. A., and Stein, E. A. (1982) Parvalbumins and other soluble high-affinity calcium-binding proteins from muscle, *Calcium Cell. Funct. 2*, 243−278.
8. Kretsinger, R. H., and Nockolds, C. E. (1973) Carp muscle calcium-binding protein. II. Structure determination and general description, *J. Biol. Chem. 248*, 3313−3326.
9. Goodman, M., and Pechère, J.-F. (1977) The evolution of muscular parvalbumins investigated by the maximum parsimony method, *J. Mol. Evol. 9*, 131−158.
10. Fohr, U. G., Weber, B. R., Muntener, M., Staudenmann, W., Hughes, G. J., Frutiger, S., Banville, D., Schafer, B. W., and Heizmann, C. W. (1993) Human alpha and beta parvalbumins. Structure and tissue-specific expression, *Eur. J. Biochem. 215*, 719−727.
11. Muntener, M., Kaser, L., Weber, J., and Berchtold, M. W. (1995) Increase of skeletal muscle relaxation speed by direct injection of parvalbumin cDNA, *Proc. Natl. Acad. Sci. U.S.A. 92*, 6504−6508.
12. Schwaller, B., Dick, J., Dhoot, G., Carroll, S., Vrbora, G., Nicotera, P., Pette, D., Wyss, A., Bluethmann, H., Hunziker, W., and Celio, M. R. (1999) Prolonged contraction-relaxation cycle of fast-twitch muscles in parvalbumin knockout mice, *Am. J. Physiol. 276*, 395−403.
13. Caillard, O., Moreno, H., Schwaller, B., Llano, I., Celio, M. R., and Marty, A. (2000) Role of the calcium-binding protein parvalbumin in short-term synaptic plasticity. *Proc. Natl. Acad. Sci. U.S.A. 97*, 13372−13377.
14. Pack, A. K., and Slepecky, N. B. (1995) Cytoskeletal and calcium-binding proteins in the mammalian organ of Corti: cell type-specific proteins displaying longitudinal and radial gradients, *Hear. Res. 91*, 119−135.
15. Henzl, M. T., Shibasaki, O., Comegys, T. H., Thalmann, I., and Thalmann, R. (1997) Oncomodulin is Abundant in the Organ of Corti, *Hear. Res. 106*, 105−111.
16. Sakaguchi, N., Henzl, M. T., Thalmann, I., Thalmann, R., and Schulte, B. A. (1998) Oncomodulin is Expressed Exclusively by Outer Hair Cells in the Organ of Corti, *J. Histochem. Cytochem. 46*, 29−39.
17. Pauls, T. L., Durussel, I., Cox, J. A., Clark, I. D., Szabo, A. G., Gagne, S. M., Sykes, B. D., and Berchtold, M. W. (1993) Metal binding properties of recombinant rat parvalbumin wild-type and F102W mutant, *J. Biol. Chem. 268*, 20897−20903.
18. Eberhard, M., and Erne, P. (1994) Calcium and magnesium binding to rat parvalbumin, *Eur. J. Biochem. 222*, 21−26.
19. Rinaldi, M. L., Haiech, J., Pavlovitc, J, Rizk, M., Ferraz, C., Derancourt, J., and Demaille, J. G. (1982) Isolation and characterization of a rat skin parvalbumin-like calcium-binding protein, *Biochemistry 21*, 4805−4810.
20. Hapak, R. C., Lammers, P. J., Palmisano, W. A., Birnbaum, E. R., and Henzl, M. T. (1989) Site-specific substitution of glutamate for aspartate at position 59 of rat oncomodulin, *J. Biol. Chem. 264*, 18751−18760.
21. Cox, J. A., Milos, M., and MacManus, J. P. (1990) Calcium- and magnesium-binding properties of oncomodulin, *J. Biol. Chem. 265*, 6633−6637.
22. Epstein, P., Means, A. R., and Berchtold, M. W. (1986) Isolation of a rat parvalbumin gene and full length cDNA, *J. Biol. Chem. 261*, 5886−5891.
23. Gillen, M. F., Banville, D., Rutledge, R. G., Narang, S., Seligy, V. L., Whitfield, J. F., and MacManus, J. P. (1987) A complete complementary DNA for the oncodevelopmental calcium-binding protein, oncomodulin, *J. Biol. Chem. 262*, 5308−5312.
24. Henzl, M. T., and Graham, J. S. (1999) Conformational stabilities of the rat α- and β-parvalbumins, *FEBS Lett. 442*, 241−245.
25. Agah, S., Larson, J. D., and Henzl, M. T. (2003) Impact of Proline Residues on Parvalbumin Stability, *Biochemistry 42*, 10886−10895.
26. Henzl, M. T., Larson, J. D., and Agah, S. (2000) Influence of monovalent cations on rat α- and β-parvalbumin stabilities, *Biochemistry 39*, 5859−5867.
27. Haner, M., Henzl, M. T., Raissouni, B., and Birnbaum, E. R. (1984) Synthesis of a new chelating gel. Removal of Ca^{2+} ions from parvalbumin, *Anal. Biochem. 138*, 229−234.
28. Henzl, M. T., Agah, S., and Larson, J. D. (2003) Characterization of the metal ion-binding domains from rat α- and β-parvalbumins, *Biochemistry 42*, 3594−3607.
29. Womack, F. C., and Colowick, S. P. (1973) Rapid measurement of binding of ligands by rate of dialysis, *Methods Enzymol. 27*, 464−471.
30. Nyhoff, L., and Leestma, S. (1995) in *Fortran 77 and Numerical Methods for Engineers and Scientists*, Prentice-Hall, Englewood Cliffs, NJ.
31. Bevington, P. R., and Robinson, D. K. (1992) in *Data Reduction and Error Analysis for the Physical Sciences*, 2nd ed., McGraw-Hill, Boston, MA.
32. Bevington, P. R. (1969) in *Data Reduction and Error Analysis for the Physical Sciences*, McGraw-Hill, Boston, MA.
33. Lacowicz, J. R. (1999) in *Principles of Fluorescence Spectroscopy*, 2nd ed., p 123, Kluwer Academic/Plenum Publishers, New York.
34. Henzl, M. T., Larson, J. D., and Agah, S. (2003) Estimation of parvalbumin Ca^{2+}- and Mg^{2+}-binding constants by global least squares analysis of isothermal titration calorimetry data, *Anal. Biochem. 319*, 216−233.
35. Mori, S., Abeygunawardana, C., Johnson, M. O., and van Zijl, P. C. M. (1995) Improved sensitivity of HSQC spectra of exchanging protons at short interscan delays using a new fast HSQC (FHSQC) detection scheme that avoids water saturation, *J. Magn. Reson. B108*, 94−98.
36. Baldellon, C., Alattia, J.-R., Strub, M.-P., Pauls, T., Berchtold, M. W., Cavé, A., and Padilla, A. (1998) ^{15}N NMR relaxation studies of calcium-loaded parvalbumin show tight dynamics compared to those of other EF-hand proteins, *Biochemistry 37*, 9964−9975.

37. Rance, M. (1987) Improved techniques for homonuclear rotating-frame and isotropic mixing experiments, *J. Magn. Reson. 74*, 557−564.
38. Muhandiram, D. R., Farrow, N. A., Xu, G., Smallcombe, S. H., and Kay, L. E. (1992) A gradient ^{13}C NOEY-HSQC experiment for recording NOESY spectra of ^{13}C-labeled proteins dissolved in H_2O, *J. Magn. Reson. B102*, 317−321.
39. Henzl, M. T., Hapak, R. C., and Likos, J. J. (1998) Interconversion of the ligand arrays in the CD and EF sites of oncomodulin. Influence on Ca^{2+}-binding affinity, *Biochemistry 37*, 9101−9111.
40. Corson, D. C., Williams, T. C., and Sykes, B. D. (1983) Calcium binding proteins: optical stopped-flow and proton nuclear magnetic resonance studies of the binding of the lanthanide series of metal ions to parvalbumin, *Biochemistry 22*, 5882−5889.
41. Williams, T. C., Corson, D. C., and Sykes, B. D. (1984) Calcium-binding proteins: calcium(II)-lanthanide(III) exchange in carp parvalbumin, *J. Am. Chem. Soc. 106*, 5698−5702.
42. Williams, T. C., Corson, D. C., Sykes, B. D., and MacManus, J. P. (1987) Oncomodulin. ^1H NMR and optical stopped-flow spectroscopic studies of its solution conformation and metal-binding properties, *J. Biol. Chem. 262*, 6248−6256.
43. Declercq, J.-P., Tinant, B., Parello, J., and Rambaud, J. (1991) Ionic interactions with parvalbumins. Crystal structure determination of pike 4.10 parvalbumin in four different ionic environments, *J. Mol. Biol. 220*, 1017−1039.
44. Baldellon, C., Padilla, A., and Cave, A. (1992) Kinetics of amide proton exchange in parvalbumin studied by ^1H 2-D NMR. A comparison of the Ca^{2+}- and Mg^{2+}-loaded forms. *Biochimie 74*, 837−844.
45. Di Cera, E. (1995) *Thermodynamic Theory of Site-specific Binding Processes in Biological Macromolecules*, Cambridge University Press, Cambridge, U.K.
46. Henzl, M. T., Wycoff, W. G., Larson, J. D., and Likos, J. J. (2002) ^{15}N nuclear magnetic resonance relaxation studies on rat β-parvalbumin and the penta-carboxylate variants, S55D and G98D, *Protein Sci. 11*, 158−173.
47. Haiech, J., Derancourt, J., Pechère, J.-F., and Demaille, J. (1979) Magnesium and calcium binding to parvalbumins: evidence for differences between parvalbumins and an explanation of their relaxing function, *Biochemistry 18*, 2752−2758.
48. Thépaut, M., Strub, M.-P., Cavé, A., Banères, J.-L., Berchtold, M. W., Dumas, C., and Padilla, A. (2001) Structure of rat parvalbumin with deleted AB domain: implications for the evolution of EF hand calcium-binding proteins and possible physiological relevance, *Proteins 45*, 117−128.
49. Colet, J. M., Makos, J. D., Malloy, C. R., and Sherry, A. D. (1998) Determination of the intracellular sodium concentration in perfused mouse liver by ^{31}P and ^{23}Na magnetic resonance spectroscopy, *Magn. Reson. Med. 39*, 155−159.
50. Efendiev, R., Bertorello, A. M., Zandomeni, R., Cinelli, A. R., and Pedemonte, C. H. (2002) Agonist-dependent regulation of renal Na^+,K^+-ATPase activity is modulated by intracellular sodium concentration, *J. Biol. Chem. 277*, 11489−11496.
51. Rose, C. R., and Ransom, B. R. (1997) Regulation of intracellular sodium in cultured rat hippocampal neurones, *J. Physiol. (London) 499*, 573−587.
52. Yeung, E. W., Ballard, H. J., Bourreau, J.-P., and Allen, D. G. (2003) Intracellular sodium in mammalian muscle fibers after eccentric contractions, *J. Appl. Physiol. 94*, 2475−2482.
53. Rose, C. R., Kovalchuk, Y., and Eilers, J. (1999) Two-photon imaging of spines and fine dendrites of central neurons, *Eur. J. Physiol. 439*, 201−207.
54. Knopfel, T., Guatteo, E., Bernardi, G., and Mercuri, N. B. (1998) Hyperpolarization induces a rise in intracellular sodium concentration in dopamine-containing cells of the substantia nigra pars compacta, *Eur. J. Neurosci. 10*, 1926−1929.
55. Friedman, J. E., and Haddad, G. G. (1994) Anoxia induces an increase in intracellular sodium in rat central neurons in vitro, *Brain Res. 663*, 329−334.
56. Raley-Susman, K. M., Kass, I. S., Cottrell, J. B., Newman, R. B., Chambers, G., and Wang, J. (2001) Sodium influx blockade and hypoxic damage to CA1 pyramidal neurons in rat hippocampal slices, *J. Neurophysiol. 86*, 2715−2726.
57. Müller, M., and Somjen, G. G. (2000) Na^+ and K^+ concentrations, intra- and extracellular voltages, and the effect of TTX in hypoxic rat hippocampal slices, *J. Neurophysiol. 83*, 735−745.
58. Thalmann, I., Thalmann, R., and Henzl, M. T. (1998) Novel calcium sensor in the outer hair cells: quantitation of oncomodulin, *Prim. Sens. Neuron 2*, 283−296.
59. Wangenmann, P., and Schacht, J. (1996) Homeostatic mechanisms in the cochlea, in *The Cochlea* (Dallos, P., Popper, A. N., and Fay, R. R., Eds.), pp 130−185, Springer-Verlag, New York.
60. Ashmore, J. F. (1987) A fast motile response in guinea-pig outer hair cells: the cellular basis of the cochlear amplifier, *J. Physiol. (London) 388*, 323−347.
61. Kachar, B., Brownell, W. E., Altschuler, R. A., and Fex, J. (1986) Electrokinetic shape changes of cochlear outer hair cells, *Nature 322*, 365−368.
62. Zheng, J., Shen, W., He, D. Z. Z., Long, K. B., Madison, L. D., and Dallos, P. (2000) Prestin is the motor protein of cochlear outer hair cells, *Nature 405*, 149−155.

BI035890K